Biogeosciences, 21, 689–709, 2024
https://doi.org/10.5194/bg-21-689-2024

Biogeosciences Open Access EGU

Latitudinal distribution of biomarkers across the western Arctic Ocean and the Bering Sea: an approach to assess sympagic and pelagic algal production

Youcheng Bai[1,2], Marie-Alexandrine Sicre[3], Jian Ren[1,2], Vincent Klein[3], Haiyan Jin[1,2,4], and Jianfang Chen[1,2,5]

[1]Key Laboratory of Marine Ecosystem Dynamics, Ministry of Natural Resources, Hangzhou 310012, China
[2]Second Institute of Oceanography, Ministry of Natural Resources, Hangzhou 310012, China
[3]LOCEAN, CNRS, Sorbonne Université, Campus Pierre et Marie Curie, Case 100, 4 Place Jussieu, 75032 Paris, France
[4]School of Oceanography, Shanghai Jiao Tong University, Shanghai 200230, China
[5]State Key Laboratory of Satellite Ocean Environment Dynamics, Second Institute of Oceanography, Ministry of Natural Resources, Hangzhou 310012, China

Correspondence: Jianfang Chen (jfchen@sio.org.cn)

Received: 28 August 2023 – Discussion started: 1 September 2023
Revised: 23 November 2023 – Accepted: 1 December 2023 – Published: 7 February 2024

Abstract. The drastic decline of Arctic sea ice due to global warming and polar amplification of environmental changes in the Arctic basin profoundly alter primary production with consequences for polar ecosystems and the carbon cycle. In this study, we use highly branched isoprenoids (HBIs), brassicasterol, dinosterol and terrestrial biomarkers (*n*-alkanes and campesterol) in surface sediments to assess sympagic and pelagic algal production with changing sea-ice conditions along a latitudinal transect from the Bering Sea to the high latitudes of the western Arctic Ocean. Suspended particulate matter (SPM) was also collected in surface waters at several stations of the Chukchi Sea to provide snapshots of phytoplankton communities under various sea-ice conditions for comparison with underlying surface sediments. Our results show that sympagic production (IP_{25} and HBI-II) increased northward between 62 and 73° N, with maximum values at the sea-ice edge in the Marginal Ice Zone (MIZ) between 70 and 73° N in the southeastern Chukchi Sea and along the coast of Alaska. It was consistently low at northern high latitudes (> 73° N) under extensive summer sea-ice cover and in the Ice-Free Zone (IFZ) of the Bering Sea. Enhanced pelagic sterols and HBI-III occurred in the IFZ across the Bering Sea and in the southeastern Chukchi Sea up to 70–73° N in MIZ conditions, which marks a shift of sympagic over pelagic production. In surface water SPM, pelagic sterols display similar patterns as chlorophyll *a*, increasing southward with higher amounts found in the Chukchi shelf, pointing to the dominance of diatom production. Higher cholesterol values were found in the mid-Chukchi Sea shelf where phytosterols were also abundant. This compound prevailed over phytosterols in sediments, compared to SPM, reflecting efficient consumption of algal material in the water column by herbivorous zooplankton.

1 Introduction

The Arctic Ocean is undergoing the most rapid climate and environmental changes of the world ocean with notably the drastic reduction of sea-ice cover and thickness and increased freshwater from higher Arctic river flows (Masson-Delmotte et al., 2021). This rapid sea-ice retreat due to global warming has major consequences not only on sea-ice ecosystems thriving in and below sea ice and their diversity, but also on pelagic phytoplankton and zooplankton communities and subsequently on the food chain (Ardyna et al., 2014; Ardyna and Arrigo, 2020). Surface freshening caused by sea-ice melting and higher river run-off induces changes of phytoplanktonic species (Park et al., 2023) thereby altering the composition, export and sequestration of organic carbon in marine sediments and ultimately the Arctic marine carbon sink (Brown et al., 2020; Coupel et al., 2015; Su et al, 2023).

In general, at the onset of the spring bloom period (April–July), diatoms and large phytoplankton are dominant, while the percentage of smaller phytoplankton increases in later summer and/or early autumn, and thus organic carbon fluxes to the sediments are mainly driven by larger phytoplankton cells (Moran et al., 2012). Li et al. (2009) evidenced a shift toward the smallest phytoplankton cells at the expense of larger cells as a result of upper water column stratification. While smaller picoplankton is efficient in using nutrients and light under stratified conditions, it is less prone to sinking due to low cell density and thus does not support large vertical export as opposed to micro-phytoplankton such as diatoms (Li et al., 2009). Such shift in the phytoplankton community need to be better assessed in order to understand the production pathways and the impact on secondary production, including microbial communities, and on higher trophic levels as well as export and sequestration of organic carbon to the deep ocean, known as "the biological pump" (Lannuzel et al., 2020).

Sea ice provides a habitat for a wide array of microalgae, bacteria and autotrophic, mixotrophic and heterotrophic protists (Gradinger, 1999; Hop et al., 2020). Ice-associated production (sympagic) is higher in the bottom of the sea ice due to the nutrient supply from the underlying seawater (Arrigo, 2017; Brown et al., 2011). Ice algae are also an important component in the transfer of organic carbon to deeper layers because they form aggregates that can sink faster (Boetius et al., 2013). Usually, they sink very fast as episodic events similar to sea-ice melting. Estimates of the contribution of sympagic production to primary production varies from 0 % to 80 % depending on the sea-ice type, region and season and are thus difficult to assess on a basin-wide level (Ehrlich et al., 2021; Gosselin et al., 1997; Legendre et al., 1992). Boetius et al. (2013) reported that in summer 2012 with an unprecedented decline of sea ice, macro-aggregates of diatom *Melosira arctica* contributed at least 45 % of total primary productivity and more than 85 % of carbon export in the central Arctic basin between 82 and 89° N. The increased area of thin seasonal sea ice and melt ponds with sea ice due to global warming is likely to affect phytoplankton carbon uptake and export. The longer season for primary production due to earlier melting and later freezing is another parameter that will most likely enhance carbon uptake in the future.

Organic biomarkers can be used to evaluate sympagic and pelagic primary production. Among them, the mono-unsaturated highly branched isoprenoid alkene (HBI), known as IP_{25} (ice proxy with 25 carbon atoms), is a well-established biomarker of sea-ice diatoms of the genera *Haslea* and *Pleurosigma* (Belt et al., 2007; Brown et al., 2014a). The diene, HBI-II, is also biosynthesized by sympagic diatoms and is generally present with IP_{25} in northern polar oceans (Belt and Müller, 2013). By contrast, the triene, HBI-III, is believed to be produced by pelagic diatoms and has subsequently been proposed as an indicator of pelagic algal production (Belt et al., 2017), partly owing to its occurrence in sediments at the sea-ice edge or under ice-free conditions in summer (Belt et al., 2015; Schmidt et al., 2018; Smik et al., 2016).

IP_{25} was initially proposed by Belt et al. (2007) as a proxy of seasonal sea ice. Since the first high-resolution reconstruction published by Massé et al. (2008) in the Nordic seas, HBIs have been extensively used in paleoceanographic studies to achieve semi-quantitative estimates of seasonal sea-ice extent (Belt, 2018 and reference therein; Kolling et al., 2020, 2023; Müller et al., 2011; Stein et al., 2016). However, few HBI studies have been conducted to assess sympagic versus pelagic production in the western Arctic Ocean and Bering Sea (Koch et al., 2020a, b). In this study, HBIs were used together with selected phytosterols to explore the relationship between sympagic–pelagic algal production and sea-ice conditions across a latitudinal transect in the Bering Sea and Chukchi Sea under rapid sea-ice decline. For this purpose, we also used earlier data from Bai et al. (2019), focused on PIP_{25} assessment, for a more complete picture of changing primary production between 54.6 and 85.4° N. Suspended particles were also collected in surface waters in summer 2014 at 13 stations for sterol analyses and compared with surface sediments to provide insight into export pathways.

2 Regional settings

The two main surface ocean currents of the Bering Sea basin are the eastward Aleutian North Slope Current (ANSC) flowing along the Aleutian Islands (Stabeno and Reed, 1994) and the Bering Slope Current (BSC) flowing along the Bering Sea slope, originating from the inflow of Alaskan Stream (AS) and driving a large-scale cyclonic circulation in the Bering Sea (Fig. 1). The main hydrological features of the Bering Sea northern shelf include the Anadyr Water (AW) originating from the BSC and the Alaska Coastal Water (ACW), while the surface hydrology of the Chukchi Sea is strongly influenced by the warm northward flowing Pacific Water (PW) entering the Arctic Ocean through the Bering Strait and the seasonal cover of sea ice both playing an important role in the ecology and community composition. The PW has an annual mean transport rate of 0.8 Sv (Roach et al., 1995; Woodgate et al., 2005) and comprises three water masses (Coachman et al., 1975): (i) the colder, saline (> 32.5) and nutrient-rich AW (Grebmeier et al., 1988; Weingartner et al., 2005) in the western side of the northern Bering Sea and Chukchi Sea; (ii) the relative warm, low-salinity (< 31.8) and nutrient-depleted ACW (Hunt et al., 2013; Woodgate and Aagaard, 2005) in the eastern side and in between the Bering Shelf Water (BSW) with moderate salinity (31.8–32.5; Woodgate et al., 2005) and nutrient levels; (iii) the seasonal southward-flowing Siberian Coastal Current (SCC) in the western Chukchi Sea that usually deflects small amounts of cold fresh waters (~ 0.1 Sv) into the central Chukchi Sea (Weingartner et al., 1999) (Fig. 1).

The northern Bering–Chukchi Sea is one of the largest marginal seas in the Arctic Ocean (Jakobsson et al., 2014) and one of the most productive areas (Arrigo and van Dijken, 2011; Hill et al., 2018). Because of continued nutrient supply from the PW, surface waters in this region maintain a high primary production both during the sea-ice melting season and ice-free waters in summer. With the retreat of sea ice, the algal production associated with sea ice (Gradinger, 2009) as well as the under-ice phytoplankton blooms (Ardyna et al., 2020; Arrigo et al., 2012; Coupel et al., 2012, 2015) provide food to higher trophic levels (Cautain et al., 2022; Ji et al., 2012; Kohlbach et al., 2016; Tedesco et al., 2019). With the thinning and retreat of sea ice triggered by global warming, the production and export of carbon from sea-ice algae in the Arctic Ocean will also become increasingly important (Ardyna and Arrigo, 2020). However, the exact implications of the drastic sea-ice reduction of the past few decades on marine ecosystems are difficult to predict because of adverse effects on phytoplankton (Harada et al., 2016; Shimada et al., 2006).

3 Material and methods

3.1 Surface sediment sampling

Surface sediment samples were recovered from the western Arctic Ocean, including the Bering Sea, the Bering–Chukchi shelf and the high Arctic Ocean. A total of 52 surface sediment samples (blue dots in Fig. 1) were collected on the RV *Xuelong* during CHINARE cruises ARC3, ARC4, ARC5 and ARC6 in 2008, 2010, 2012 and 2014, respectively, and analyzed for biomarkers. In addition, 36 samples obtained during the CHINARE cruises between 2008 and 2014 mostly located in the Chukchi Sea and published by Bai et al. (2019) (red dots in Fig. 1) were also used in this study. The total sample set of 88 surface sediments encompasses a latitudinal range from 54.6 to 85.4° N. Details of sampling locations are provided in Table S1 in the Supplement. All surface sediment sampling was carried out using a box corer. After the box corer was retrieved, the uppermost 0–2 cm of sediment was sliced on board and then placed in a plastic bag and stored at −20 °C until further processing.

3.2 Suspended particles sampling

Suspended particulate matter (SPM) was obtained from the filtration of surface seawater at depths ranging from 0 to 5 m during the summer cruise of the RV *Xuelong* in 2014. A Large Volume Water Transfer System (WTS-LV, Mclane) was used to perform in situ filtration of seawater (40–60 L) using glass fiber filters (Whatman GF/F, 142 mm diameter) pre-combusted at 450° for 4 h. After filtration, the particulate-laden filters were stored at −20 °C until biomarker analysis. The 13 stations occupied in the Chukchi shelf and Canada basin in summer 2014 (29 July–14 August) are shown in Fig. 1 (orange triangles).

Water samples were also collected for chlorophyll *a* (Chl *a*) analysis using 1 L Niskin bottles during the same summer 2014 cruise on the RV *Xuelong*. Surface water (0.5–1 L) was first filtered through 200 µm Nitex filters to remove zooplankton and then sequentially filtered through GF/F filters (Whatman GF/F, 25 mm diameter).

3.3 Total organic carbon (TOC) and total nitrogen (TN) sediment analyses

Approximately 1 g of freeze-dried and homogenized sediment was acidified with 1 M hydrochloric acid (HCl) and heated in a water bath at 50° for at least 48 h to remove inorganic carbon. Samples were then rinsed with milli-Q grade water until a neutral pH was reached (pH = 7) and freeze-dried to remove water (Su et al. 2023; Williford et al., 2007). The TOC and TN contents of the surface sediments were measured using an element analyzer (FLASH 2000 CHNS-O, Thermo Fisher). BBOT standard of Thermo Scientific (carbon % 72.53 %; nitrogen % 6.51 %) were used for quality control. BBOT standard was measured every eight samples to correct for drift. The standard deviation of the measurements is less than < 0.1 %.

3.4 Sample preparation and biomarker extraction

Wet SPM filters and surface sediments were freeze-dried prior to extraction. Lipids were extracted from freeze-dried SPM and from ca. 1–5 g of homogenized sediments using a mixture of dichloromethane/methanol (2 : 1, v/v). Sediment extraction was performed in a clean glass vial for 10 min in an ultrasonic bath, which was then centrifuged for 2 min at 2500 rpm. The supernatant containing the lipids was recovered with a clean glass pipette and transferred in a pre-combusted 8 mL glass vial. This operation was repeated twice and the three extracts were combined and dried under a gentle nitrogen stream. For filters, each freeze-dried sample with SPM was cut into small pieces using solvent-rinsed scissors and extracted following the same method as for the sediments. Total lipid extracts were then separated into *n*-alkanes, HBIs and sterols by silica gel chromatography using *n*-hexane, *n*-hexane/ethyl acetate (90 : 10 v/v) and *n*-hexane/ethyl acetate (70 : 30 v/v), respectively. About 50 µL BSTFA (bis-trimethylsilyl-trifluoroacetamide) was added to the sterol fractions to convert them into their corresponding trimethylsilyl ethers by heating at 70 °C for 1 h to complete derivatization before analysis by gas chromatography (GC) on an Agilent Technologies 7890 gas chromatograph coupled to a mass spectrometer (MS) Agilent 262 Technologies 5975C inert XL using a mass selective detector.

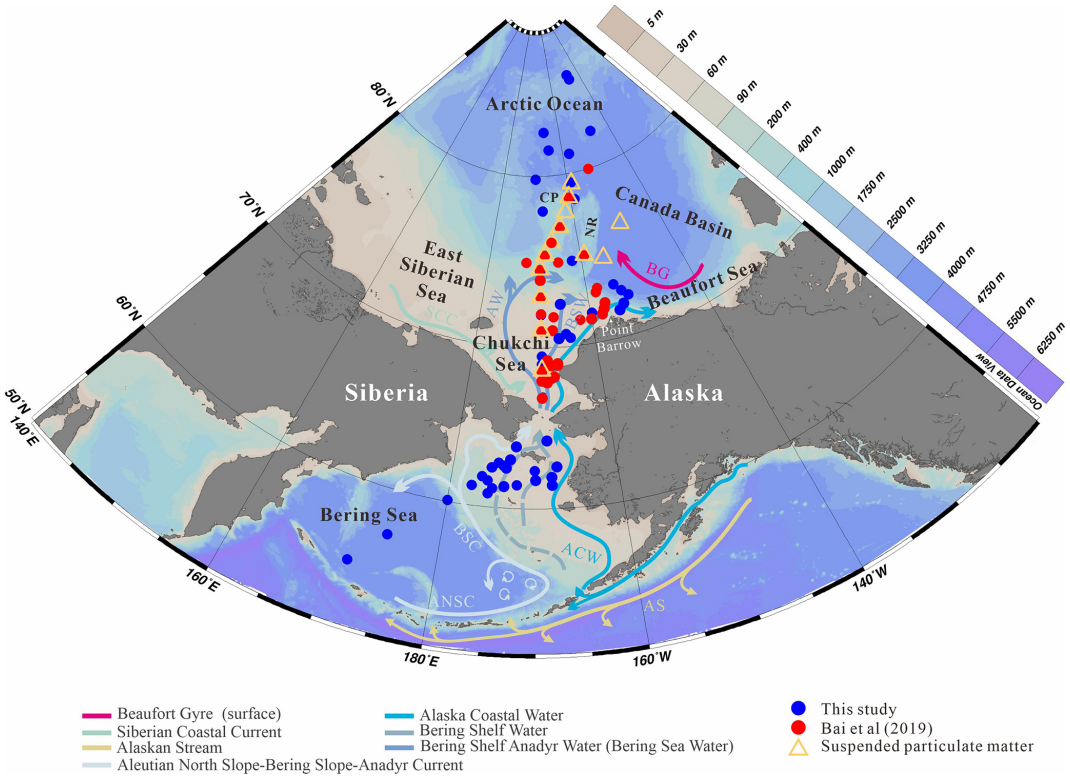

Figure 1. Map showing the location of the 88 surface samples in the Bering Sea and western Arctic Ocean, which includes the new data generated in this study (blue dots) and earlier data published by Bai et al. (2019) (red dots). Orange triangles indicate the sites where surface suspended particulate matter was collected (this study). Arrows show oceanic surface currents (after Grebmeier et al., 2006). AS, Alaskan Stream; ACW, Alaska Coastal Water; ANSC, Aleutian North Slope Current; BSC, Bering Slope Current; SCC, Siberian Coastal Current; AW, Anadyr Water; BSW, Bering Shelf Water; BG, Beaufort Gyre; CP, Chukchi Plateau; NR, Northwind Ridge. The study area covered the Bering Sea, Chukchi shelf (water depths < 140 m) and the slope and basin of the western Arctic Ocean (water depths > 140 m).

3.5 Biomarker analysis

C_{25}-HBIs (IP_{25}, HBI-II, and HBI-III) were analyzed by GC/MS. We used an HP-5MS capillary column (30 m long, 0.25 mm i.d., 0.25 µm film thickness) and an oven temperature program from 40 to 300 °C at a heating rate of 10 °C min^{-1} with a 10 min hold time at final temperature. The operating conditions for the MS were 250 °C for the ion source temperature and 70 eV for the ionization energy. HBIs were identified by comparing their GC retention times and mass spectra. A known amount of 7-hexylnonadecane (m/z 266) was added as an internal standard prior to extraction for HBI quantification. Selective ion monitoring (SIM) was performed to detect and quantify IP_{25} (m/z 350), HBI-II (m/z 348) and HBI-III Z isomers (m/z 346).

Sterols and n-alkanes were analyzed by GC using a Varian 3300 equipped with a septum programmable injector (SPI) and a flame ionization detector (FID). For n-alkanes, the oven temperature was programmed from 80 to 300 °C at a heating rate of 8 °C min^{-1} and the final temperature was held for 20 min. A 30 m long DB-5MS fused silica capillary column (0.25 mm i.d., 0.25 µm film thickness) was used for both compound classes. For sterols, the GC oven was programmed from 50 to 100 °C (30 °C min^{-1}), then from 100 to 150 °C (1.5 °C min^{-1}) and to 300 °C (3 °C min^{-1}) and held for 20 min. In both cases, a known amount of 5α-cholestane was added to the sample prior to GC analysis as an external standard for quantitation. All biomarker sediment concentrations were normalized to TOC.

3.6 H-Print index

In their original work, Brown et al. (2014b) defined HBI-fingerprint as the proportion of seven identified HBIs (in %) produced by pelagic and sympagic diatoms. The first H-Print index was proposed by Brown and Belt (2017) as the ratio of the relative proportion of pelagic and sympagic HBIs. A simplified calculation of H-Print (Eq. 1) was proposed for sediments or marine ecosystems in the Arctic using the three following HBIs (Koch et al., 2020a, b, and 2023; Su et al., 2023), IP_{25}, HBI II and HBI III, determined by GC-MS:

$$\text{H-Print}\,\% = \frac{[\text{HBI}-\text{III}]}{[\text{IP}_{25}]+[\text{HBI}-\text{II}]+[\text{HBI}-\text{III}]} \times 100. \quad (1)$$

Low values of H-Print % are indicative of higher relative sympagic production while high values reflect prevailing pelagic algae producers. This index was used as an additional information source together with phytosterols to assess phytoplankton production patterns in relation to sea-ice conditions.

3.7 Chlorophyll *a* analyses

After collection, filters for Chl *a* analysis were extracted with 10 mL of 90 % acetone at −20° in the dark for 24 h and measured using a trilogy laboratory fluorometer (10-AU, Turner Designs), which was calibrated before analysis (Holm-Hansen et al., 1965; Welschmeyer, 1994). The precision of the measurements is 0.02 mg m^{-3}.

3.8 Sea-ice distribution data

Satellite sea-ice concentrations in the study region measured from Nimbus-7 SMMR and DMSP SSM/I-SSMIS passive microwave sensors were averaged between 1994 and 2014 (Fig. 2a–d). These data were retrieved from the National Snow and Ice Data Center (NSIDC) (DiGirolamo et al., 2022). Figure 2 shows the seasonal distributions of the sea-ice extent in spring (April–June) and summer (July–September) as well as in March and September. Also shown are the 15 % and 80 % isolines that indicate that the summer Ice-Free Zone (IFZ < 15 % of sea ice) was on average located as far north as 72° N and that the Marginal Ice Zone (MIZ, sea-ice cover from 15 % to 80 %) reached 80° N latitude. However, it must be kept in mind that our surface sediment dataset covers the nearshore, shelf, and basin regions, with different deposition rates. The first 2 cm surface sediments may represent a longer time interval (decades to centuries) than modern satellite data (Pearce et al., 2017; Polyak et al., 2009; Stein et al., 2010).

3.9 Description of ODV

The distributional maps of TOC, TN and biomarker concentrations were generated with the Ocean Data View software package, version 5.6.5 (ODV, odv.awi.de, Schlitzer, 2023). They were created using the DIVA (Data Interpolating Variational Analysis) display styles gridding to represent sea-ice data from NSIDC and with the colored dots to visualize biomarker data.

4 Results

4.1 Total organic carbon and total nitrogen in surface sediments

TOC values of surface sediments vary from 0.1 % to 2.2 % (1.03 ± 0.63 %, $n = 52$) with the highest values localized in the mid-Chukchi Sea Shelf and Bering Sea, and the lowest ones at latitudes > 75° N (Fig. 3a) (Table S1). The Bering Strait exhibits relatively low TOC content. The spatial distribution of TN shows similar patterns with values ranging from 0.01 % to 0.29 % (0.14 ± 0.07 %, $n = 50$) (Fig. 3b), e.g., 1 order of magnitude lower than TOC, which results in C/N ratios of about 8 to 10 at all sites except for some of the northernmost sites that have C/N values roughly 2 times lower (Fig. 3c).

4.2 C_{25} highly branched isoprenoid (HBI) alkenes in surface sediments

The sea-ice biomarker IP_{25} was identified in 47 out of the 52 new surface sediments analyzed in this study (Fig. 4a). IP_{25} was absent (or below the detection limit) at locations in the southern Bering Sea or at the highest latitude sites between 78 and 82° N. Concentrations were generally higher in the northeast Chukchi Sea and Barrow Canyon than in the Chukchi Plateau and low in high-latitude areas where sea ice is perennial. Predominantly ice-free regions such as the Bering Sea slope and shelf also show relatively low IP_{25} contents (0.05–1.68 µg g^{-1} TOC, 0.39 ± 0.41 µg g^{-1} TOC). HBI-II was also present in most of the sediment extracts (49 out of 52). Its spatial distribution shared similar features as IP_{25}, with higher values matching those of IP_{25} (HBI-II: 0.06–3.02 µg g^{-1} TOC, 0.61 ± 0.63 µg g^{-1} TOC; Fig. 4b) and the lowest values at the highest latitudes and in most of the Bering Sea sites.

HBI-III was present in 45 out of 52 of the sediment extracts. In contrast to IP_{25} and HBI-II, the highest abundance (> 0.17 µg g^{-1} TOC) was encountered in the northern Bering Sea and at some sites of the northeast Chukchi Sea where variable sea-ice conditions prevailed in summer (Fig. 2d) and which were free of ice in September (Fig. 2b), as expected from HBI-III producers preferably growing in the sea-ice edge to ice-free waters (0.01–0.94 µg g^{-1} TOC, 0.17 ± 0.22 µg g^{-1} TOC; Fig. 4c). These results are consistent with a pelagic phytoplankton origin for this biomarker (Bai et al., 2019; Belt et al., 2015; Koch et al., 2020a, b; Su et al., 2022) and reflected by H-Print % indicating the highest values in the northern Bering Sea gradually decreasing northward with increasing seasonal sea-ice cover, e.g., the lowest value was at MIZ about 73° N, with a slight increase northward from the Chukchi border to high latitudes under extensive sea ice (Fig. 4d).

4.3 Sterols in surface sediments

Figure 5 shows the spatial distribution of prevailing and commonly used sterols in marine settings to identify phytoplankton communities. They include pelagic phytosterols, e.g., brassicasterol (24-methylcholesta-5,22(E)-dien-3β-ol) a common sterol mainly produced by marine diatoms thriving in open water in the Arctic Ocean, although in some cases this sterol may also have a riverine and/or lacustrine

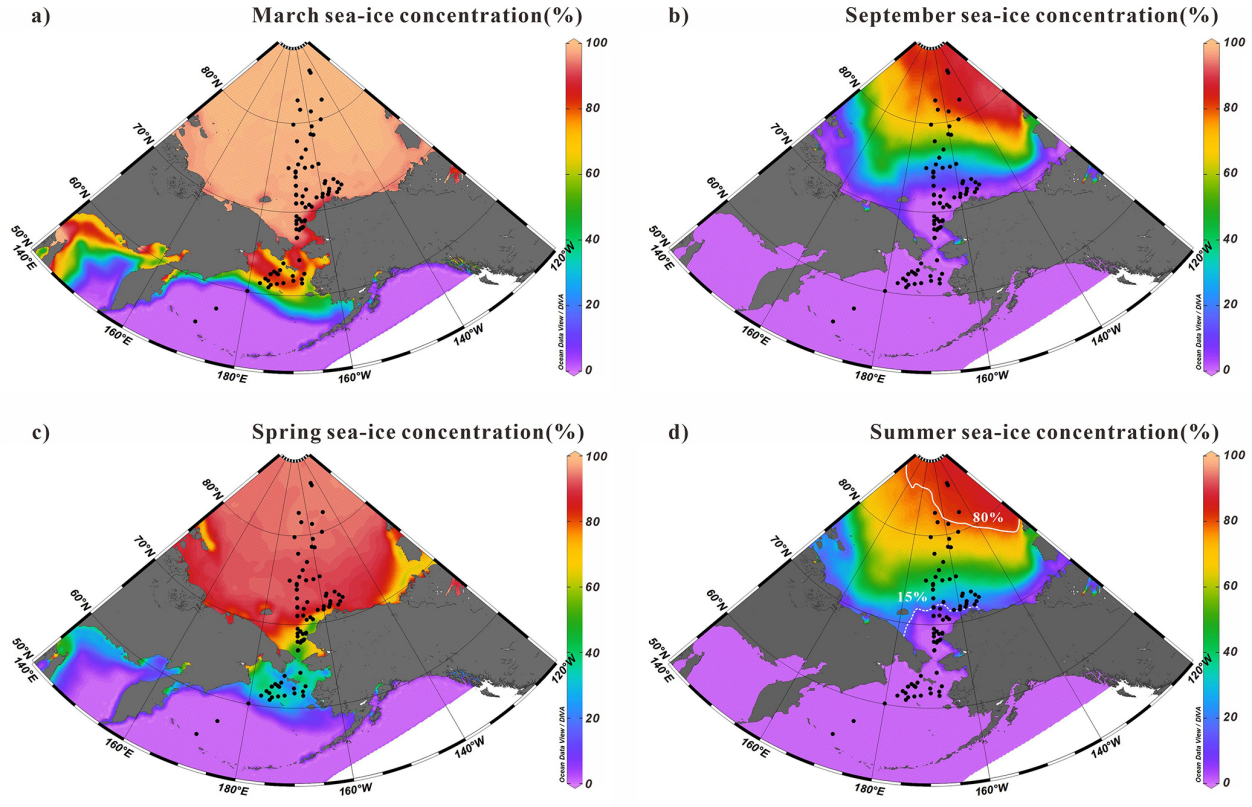

Figure 2. Average sea-ice concentrations in **(a)** March, **(b)** September, **(c)** spring (April, May and June) and **(d)** summer (July, August and September) from 1994 to 2014 (https://nsidc.org/home, last access: 14 November 2023). Black dots are surface sediment samples in this study. The dotted and solid white lines represent the 15 % and 80 % isolines, respectively, of summer sea-ice cover for the period 1994–2014.

algal origin (Fahl and Stein, 1999; Xiao et al., 2015), dinosterol (4α-23,24-trimethylcholest-22(E)-en-3β-ol) mainly synthesized by dinoflagellates but absent in sea ice, campesterol (24-methylcholest-5en-3β-ol) of terrestrial origin, and 24-ethylcholest-5-en-3β-ol, which depending on the configuration of C_{24} can be of marine (α isomer) or terrestrial (β isomer) origin (Volkman, 2016).

Concentrations of brassicasterol range from 0.72 to 57.67 $\mu g\,g^{-1}$ TOC ($7.92 \pm 10.62\,\mu g\,g^{-1}$ TOC) with the highest values found in the northern Bering Sea (57.67 $\mu g\,g^{-1}$ TOC) and southeastern Chukchi Sea shelf (0.72–37.56 $\mu g\,g^{-1}$ TOC) (Fig. 5a). Dinosterol concentrations vary in a relatively similar range, from 0.61 to 43.04 $\mu g\,g^{-1}$ TOC, around a slightly higher mean value ($14.92 \pm 11.77\,\mu g\,g^{-1}$ TOC). The distribution pattern of dinosterol shows similar features to brassicasterol with high values in the mid-Chukchi Sea shelf and northern Bering Sea but expanding further south (Fig. 5b). Campesterol and 24-ethylcholest-5-en-3β-ol show high values notably along the coast of Alaska and decrease off-shore across the Bering Strait (campesterol: 0.47–123.41 $\mu g\,g^{-1}$ TOC ($30.88 \pm 31.36\,\mu g\,g^{-1}$ TOC); 24-ethylcholest-5-en-3β-ol ranges from 0.67 to 152.35 $\mu g\,g^{-1}$ TOC ($39.52 \pm 42.08\,\mu g\,g^{-1}$ TOC)) (Fig. 5c, d). These sterols were also both present at low levels at the lowest and highest latitudes.

4.4 *N*-alkanes in surface sediments

The homologous distribution of *n*-alkanes in our sediments display an odd-to-even predominance characteristic of epicuticular waxes produced by higher plants (Yunker et al., 1995). The sum of the concentrations of high-molecular-weight odd-numbered carbon chain *n*-alkanes (C_{27}, C_{29} and C_{31}) was calculated to assess terrestrial inputs to surface sediments. The $\sum C_{27}$-C_{31} values shown in Fig. 6 vary from 11.67 to 211.86 $\mu g\,g^{-1}$ TOC ($84.16 \pm 43.44\,\mu g\,g^{-1}$ TOC) with higher contents in the southeastern Chukchi Sea shelf across the Bering Strait until the north Bering Sea. Moderate values (> 100 $\mu g\,g^{-1}$ TOC) were found at some sites of the high Arctic.

4.5 Sterols and Chl *a* in surface suspended particles

Figure 7 shows the sterol concentrations measured in surface suspended particles collected at 13 stations located along a latitudinal transect between 68.6 and 79.4° N (orange triangles in Figs. 1 and 7f). They include brassicasterol, dinosterol, 24-ethylcholest-5-en-3β-ol and cholest-5-

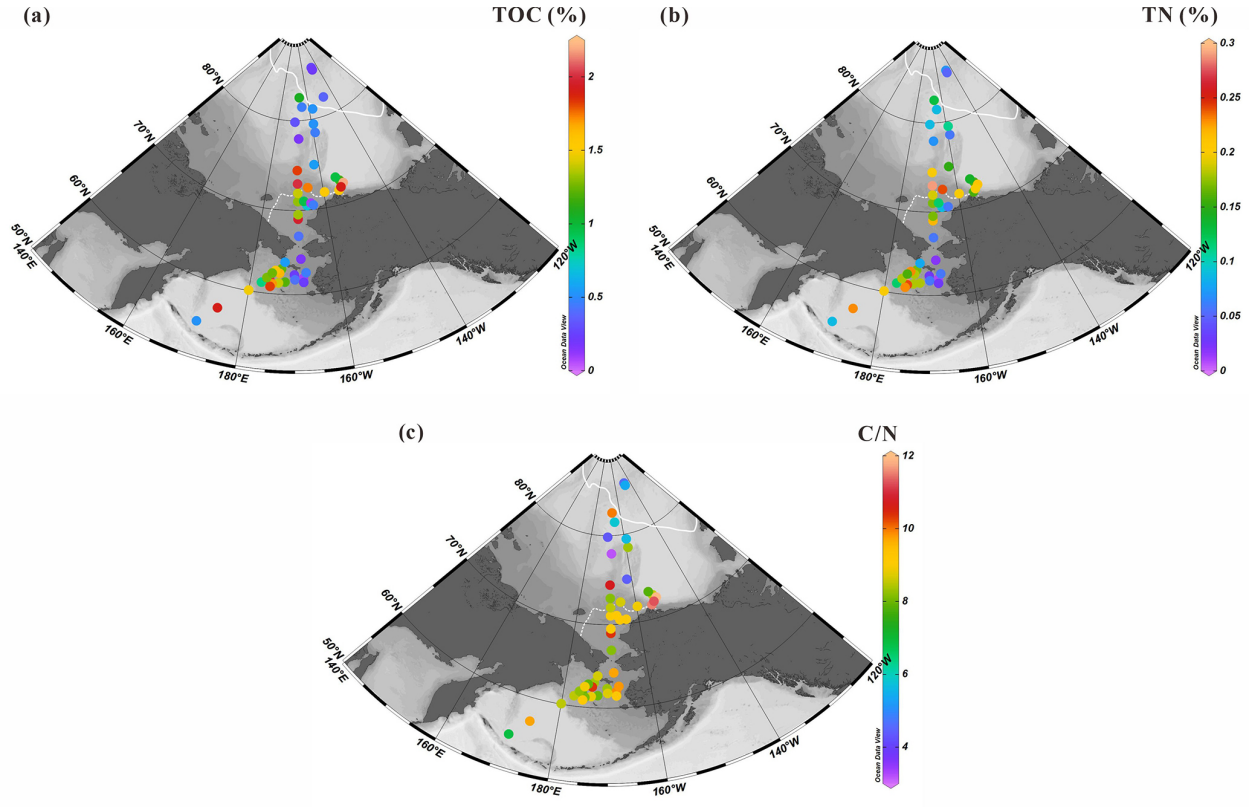

Figure 3. Distributions of **(a)** total organic carbon (TOC) in %, **(b)** total nitrogen (TN) in % and **(c)** C/N ratios in the surface sediments from the western Arctic Ocean, the Chukchi Sea and the Bering Sea (this study). For an explanation of the dotted and solid white lines, see Fig. 2.

en-3β-ol (cholesterol). Note that neither HBIs nor campesterol were detected in SPM samples indicating their absence or trace levels, below the detection limit. Concentrations of brassicasterol ranged from 0.80 to 132.31 ng L^{-1}, 17.11 $\pm$ 37.46 ng L^{-1}) (Table S3) with the highest values found in the mid-Chukchi Sea shelf where Chl *a*also reached the highest values and the lowest ones north of 75° N (Fig. 7a). Dinosterol concentrations have a much lower range from 0.51 to 17.11 ng L^{-1} (4.07$\pm$5.39 ng L^{-1}) and display similar trends as brassicasterol (Fig. 7b). Likewise, 24-ethylcholest-5-en-3β-ol also shows increased concentrations southward spanning from 1.88 to 46.04 ng L^{-1} (9.11 $\pm$ 12.13 ng L^{-1}) (Fig. 7c). Finally, cholesterol, one of the most abundant sterols in SPM, varied from 1.20 to 117.29 ng L^{-1} (17.02 $\pm$ 32.04 ng L^{-1}) in a range that is similar to brassicasterol (Fig. 7d). Despite possible algal sources, cholesterol is considered to mainly reflect the presence of zooplankton as it converts much of the sterols produced by algae into cholesterol. Chl *a* in surface waters shows the same south-to-north latitudinal decrease with concentrations spanning from 0.05 to 5.40 mg m^{-3} (0.69 $\pm$ 1.66 mg m^{-3}) (Fig. 7e).

5 Discussion

5.1 Impact of sea ice on sedimentary HBI distribution

In this section, we discuss the spatial distribution of HBIs based on the compilation of the sedimentary data from the CHINARE cruises ARC3, ARC4, ARC5 and ARC6 in the Chukchi Sea and Bering Sea (this study) and those from the CHINARE cruises ARC3, ARC5 and ARC6 published by Bai et al. (2019) obtained following the same analytical procedure (Fig. 8).

Sympagic IP_{25} and HBI-II values of the combined dataset range from 0.05 to 4.39 µg g^{-1} TOC (0.45 $\pm$ 0.61 µg g^{-1} TOC) and from 0.06 to 4.46 µg g^{-1} TOC (0.66 $\pm$ 0.75 µg g^{-1} TOC), respectively (Fig. 8a, b, Table S2). These values are close to those reported by Bai et al. (2019) spanning from 0.09 to 4.39 µg g^{-1} TOC (0.52$\pm$0.80 µg g^{-1} TOC) and from 0.12 to 4.46 µg g^{-1} TOC (0.72 $\pm$ 0.89 µg g^{-1} TOC) for IP_{25} and HBI-II, respectively. They confirm the extreme values off the Alaskan coast and provide new lower extremes in the Bering Sea slope and shelf, not included in the study by Bai et al. (2019), where ice-free conditions prevail in summer (Fig. 8a, b). The strong correlation between sedimentary IP_{25} and HBI-II ($r^2 = 0.87$, $p < 0.05$, Fig. S1) agrees with these two structural homologues having common sources in the

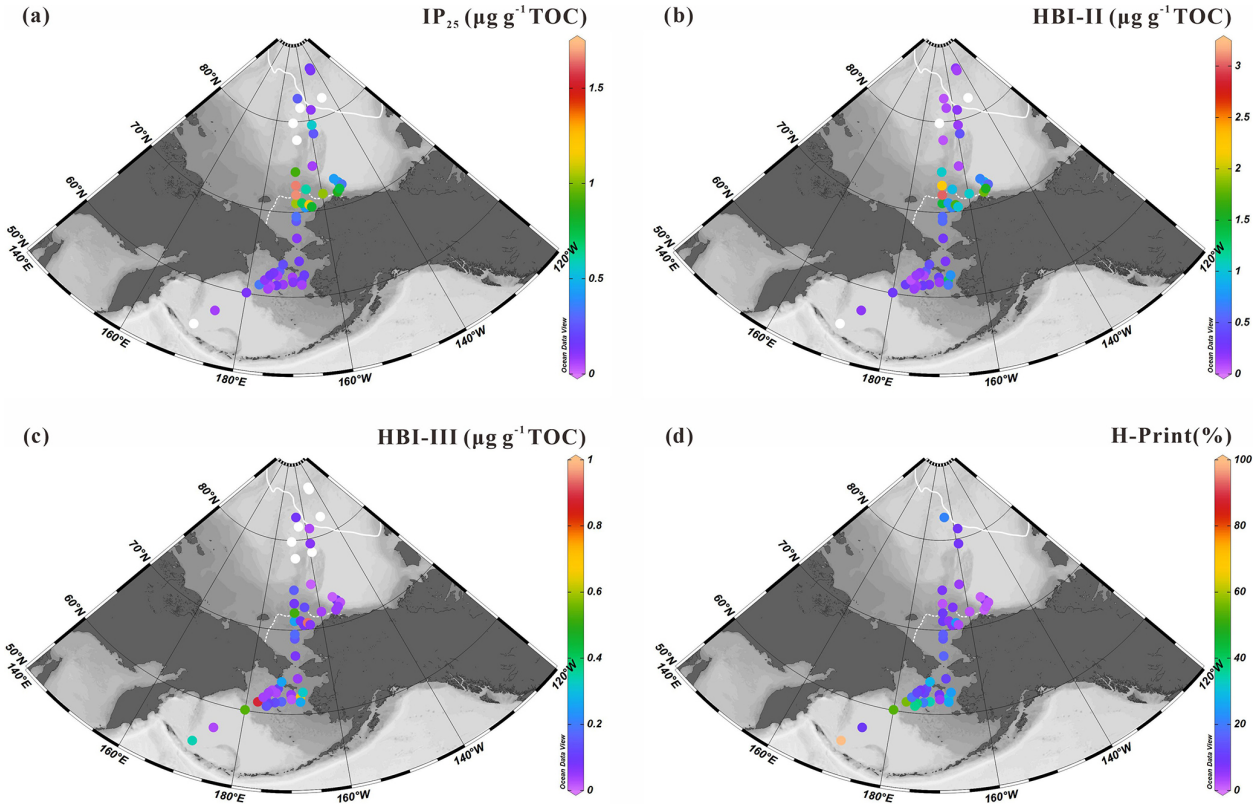

Figure 4. Surface sediment concentrations of HBIs normalized to TOC (expressed in µg g^{-1} TOC): **(a)** IP_{25}, **(b)** HBI-II, **(c)** HBI-III; **(d)** values of H-Print % of the western Arctic Ocean, the Chukchi Sea and the Bering Sea (this study). White dots are sites where HBIs were not detected. For an explanation of the dotted and solid white lines, see Fig. 2.

Arctic Ocean and northern North Atlantic (Belt, 2018) and with the presence of HBI-II in each IP_{25}-producing species studied by Brown et al. (2014a). Overall, the distribution patterns of sympagic IP_{25} and HBI-II in the augmented dataset confirms the earlier finding of low values at latitudes > 73° N due to extensive sea-ice cover in summer and provide new low end-member values south of the Bering Strait essentially free of ice in summer. Enhanced sympagic production is generally found on the path of the warm polarward PW and ACW flowing along the coast of Alaska, both contributing to ice melting. A comparison with other published data shows that our IP_{25} values are lower than reported in the Chukchi Plateau and basin by Xiao et al. (2015), lying between 0.63 and 8.97 µg g^{-1} TOC, a result that is explained by the generally more northern position of their sites and possibly also different quantification methods. The lowest IP_{25} reported by Méheust et al. (2013) (0.079–0.567 µg g^{-1} TOC) in a few (3 out of 11) surface sediments of the Bering Sea are also in agreement with our results and expected from seasonal sea ice in the Bering Sea shelf break, north of the March sea-ice edge (20% isoline in Méheust et al., 2013). The northward latitudinal decrease of IP_{25} in surface sediments and elevated values around 70° N were also reported by Koch et al. (2020a).

The distribution pattern of pelagic HBI-III is expectedly different from that of sympagic HBIs and exhibits much lower abundances (0.01–0.94 µg g^{-1} TOC, 0.16 ± 0.21 µg g^{-1} TOC) (Fig. 8c, Table S2). HBI-III is absent or present in trace amounts mostly in ice-covered areas of the high Arctic and is highest at summer ice-free sites of the northern Bering Sea (Station 10BB01, 0.89 µg g^{-1} TOC, Table S2). Elevated concentrations occurred in the southeastern Chukchi Sea shelf along the coast of Alaska, as also found by Koch et al. (2020a), and in the Bering Sea. These observations translate into H-Print index values indicating that pelagic-to-sympagic diatom production and export increases from north to south across the Bering Strait and further in the northern Bering Sea (Fig. 8d). This result is consistent with previous findings in the Pacific Arctic surface sediments by Koch et al. (2020b).

Advective processes linked to the PW flow and their impact on sea-ice dynamics in shaping algal communities have been invoked to explain sympagic-to-pelagic spatial distribution. The rate of sea-ice retreat in the Chukchi Sea is closely connected to heat transport by the PW triggering the onset of sea-ice melting in spring and/or summer. Time series from a year-round mooring deployed in the Bering Strait has shown that the annual mean transport volume of PW

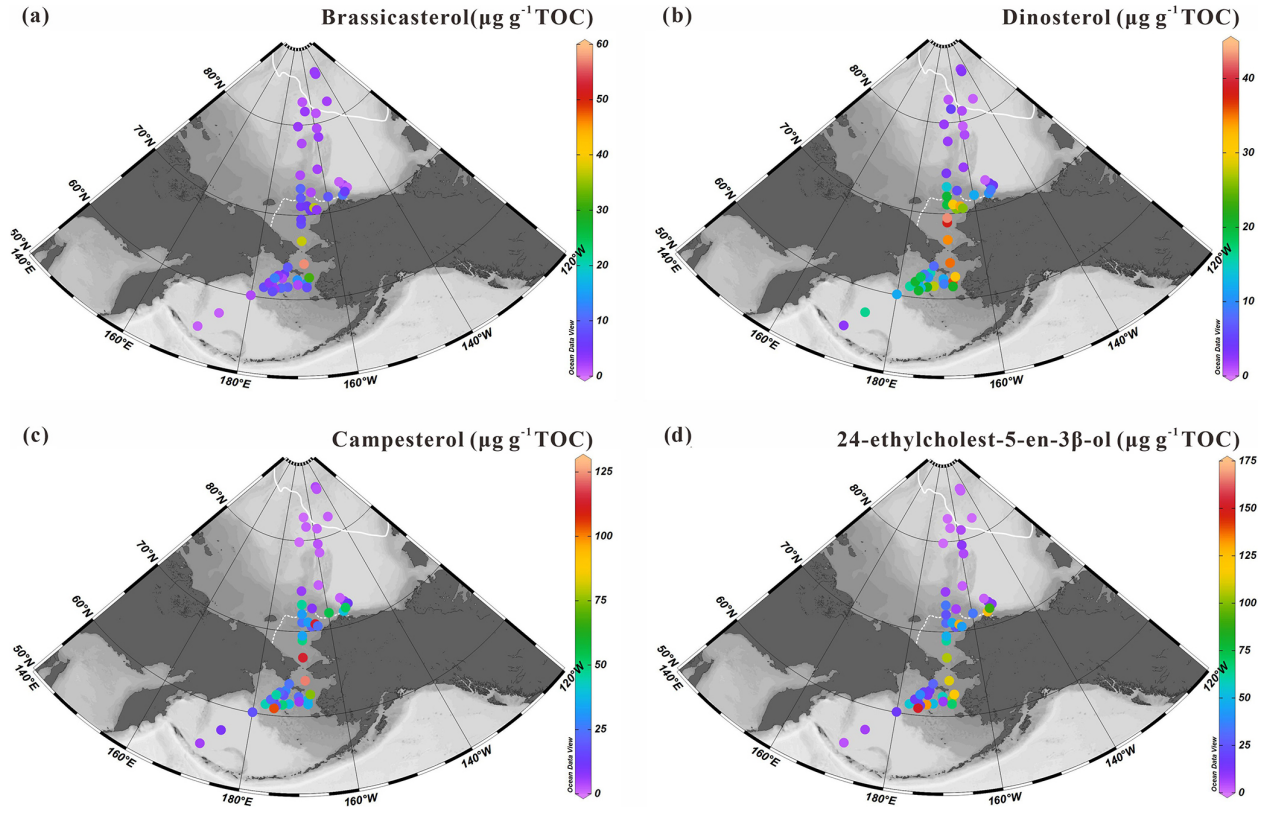

Figure 5. Concentrations of sterols expressed in $\mu g\,g^{-1}$ TOC: **(a)** brassicasterol, **(b)** dinosterol, **(c)** campesterol and **(d)** 24-ethylcholest-5-en-3β-ol in surface sediments from the western Arctic Ocean, the Chukchi Sea and the Bering Sea (this study). For an explanation of the dotted and solid white lines, see Fig. 2.

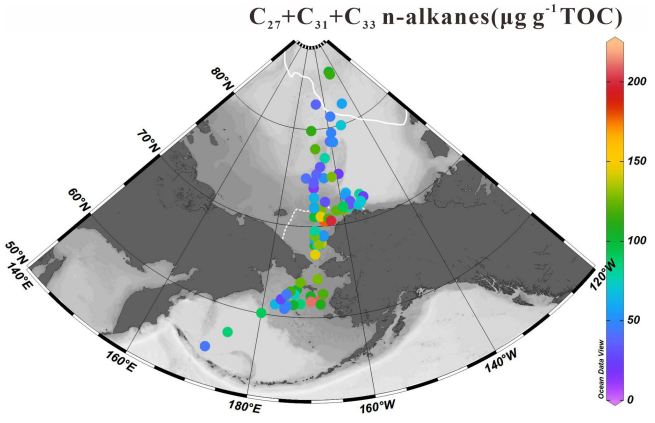

Figure 6. Sum of terrigenous long-chain odd-numbered $C_{27}+C_{29}+C_{31}$ n-alkanes (expressed in $\mu g\,g^{-1}$ TOC) in surface sediments ($n = 88$) from the western Arctic Ocean, the Chukchi Sea and the Bering Sea (this study). For an explanation of the dotted and solid white lines, see Fig. 2.

increased by $\sim 70\,\%$ between 2001 and 2014 (Woodgate, 2018). Woodgate and Peralta-Ferriz (2021) further calculated an increase of 0.1 Sv yr^{-1} between 1990 and 2019 and a corresponding $\sim 0.1\,°C\,yr^{-1}$ warming in spring and/or summer over this time interval. These authors also outlined that concomitantly the warm period extended from 5.5 to 7 months. This is in contrast with the Bering Sea, which has not shown any significant long-term reduction since 1850, despite a general warming climate, but pronounced decadal scale variability (Walsh et al., 2017) driven by the Pacific Decadal Oscillation (PDO), the dominant mode of atmospheric variability in the North Pacific.

Overall, based on the sedimentary distribution of HBIs and their translation into H-Print, we were able to discriminate the three following sub-regions (Fig. 9): (i) the Bering Sea characterized by high variability of pelagic-to-sympagic production reflecting a wide range of sea-ice conditions with sea ice forming in winter and ice-free conditions in summer (Walsh et al., 2017); (ii) the productive MIZ waters of the mid-Chukchi Sea shelf with higher sympagic production and export, and lower spread associated with variable seasonal sea-ice conditions; (iii) the slope and western Arctic Ocean basin characterized by dominating sympagic pro-

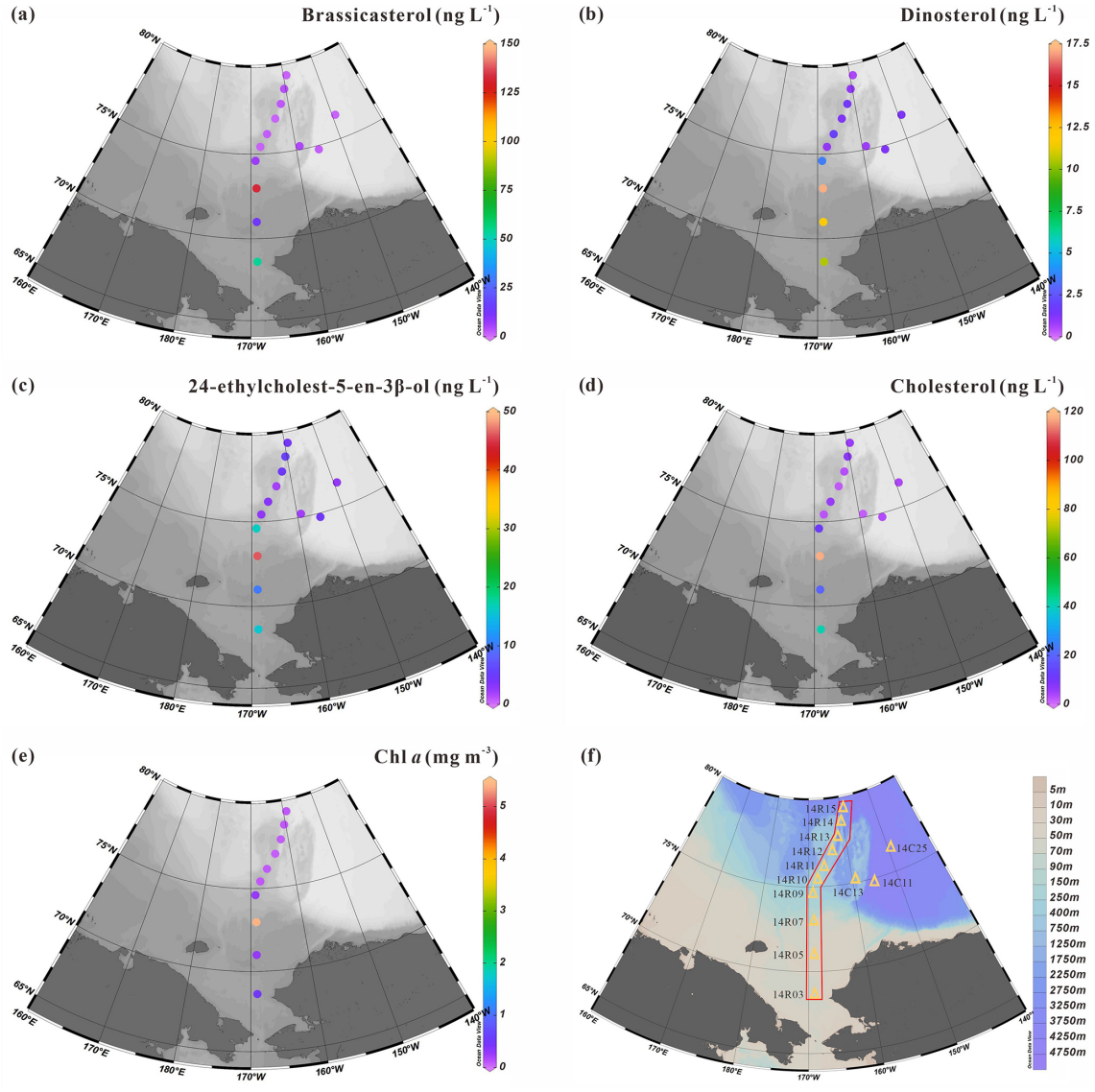

Figure 7. Distribution of biomarker sterols (in ng L^{-1}) and chlorophyll *a* (in mg m^{-3}) in surface suspended particles collected in summer 2014: **(a)** brassicasterol, **(b)** dinosterol, **(c)** 24-ethylcholest-5-en-3β-ol, **(d)** cholesterol, **(e)** Chl *a*. **(f)** Transect showing 10 of 13 stations from the shelf to the basin in the Chukchi Sea where suspended particulate matter was collected.

duction and slightly less variability reflecting prevailing high sea-ice cover.

5.2 Latitudinal variations of sympagic-to-pelagic phytoplankton production

In order to explore further the relationship between the icescape and sympagic-to-pelagic production across the wide range of sea-ice situations encountered from the Bering Sea to the high Arctic Ocean, phytosterols (brassicasterol + dinosterol) in surface sediments were investigated and compared with spring and summer sea-ice concentrations provided by the NSIDC (Fig. 10a). As shown in Fig. 10b, sympagic production increased from 62 to 70° N to reach maximum values near the sea-ice edge and MIZ, between 70 and 73° N, and decreased to low values similar to the IFZ at latitudes $> 73°$ N as sea ice became permanent. By contrast, enhanced pelagic phytosterols and HBI-III largely prevailed in open waters of the Bering Sea in spring and summer and decreased relative to sympagic production in the MIZ, demonstrating a progressive transition of habitats.

This biogeographic pattern is supported by surface sediment data of Koch et al. (2020a) retrieved from the Distribution Biological Observatory (DBO) regions surveyed during several cruises from 2012 to 2017 (Moore and Grebmeier et al., 2018) where abundances of IP_{25} in the northeast Chukchi Sea and Barrow Canyon (71–72.5° N) prevailed over those

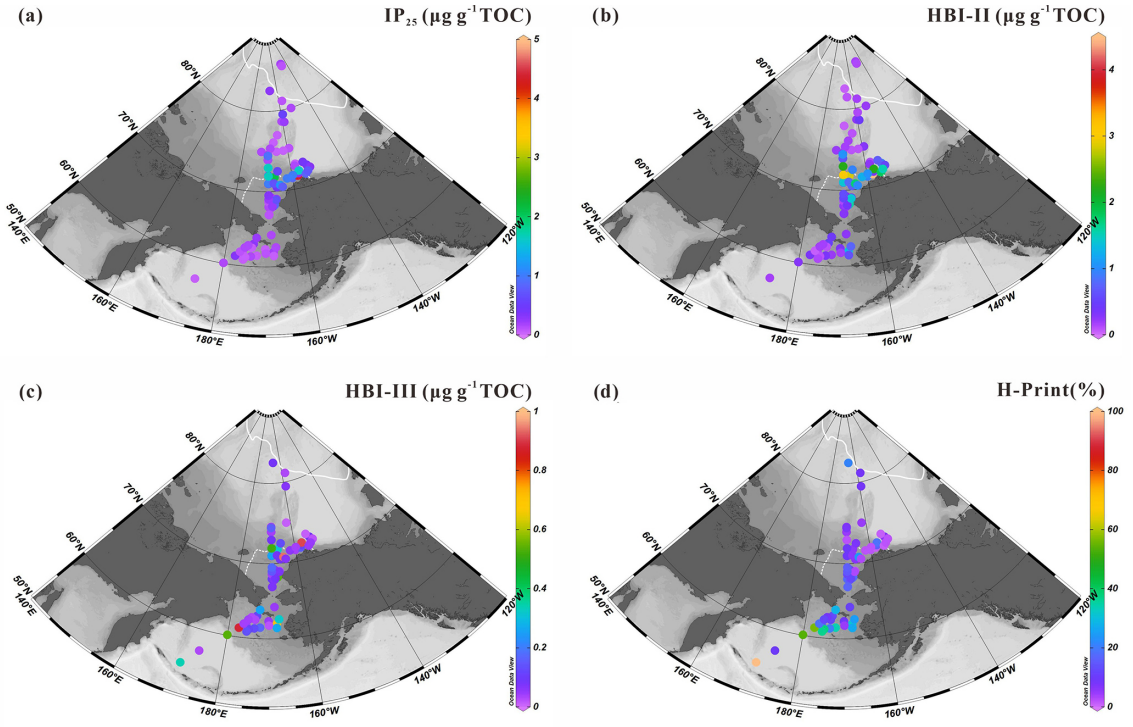

Figure 8. Surface sediment concentrations of HBIs normalized to TOC (expressed in µg g^{-1} TOC): **(a)** IP_{25}, **(b)** HBI-II, **(c)** HBI-III; **(d)** values of H-Print % in the sites ($n = 88$) of the western Arctic Ocean, the Chukchi Sea and the Bering Sea. For an explanation of the dotted and solid white lines, see Fig. 2.

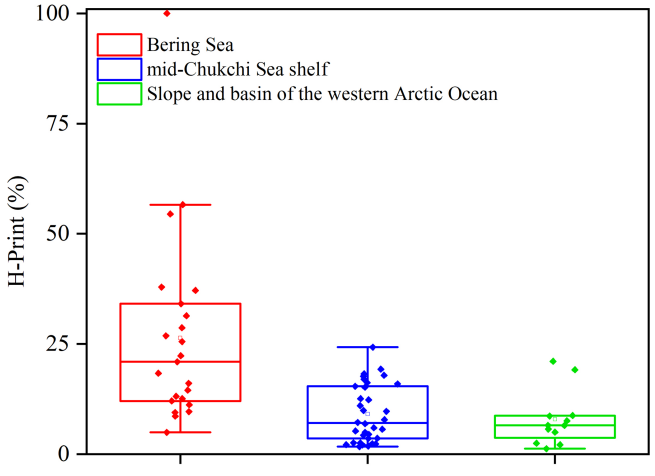

Figure 9. Boxplot of H-Print index in surface sediments from the Bering Sea (in red), mid-Chukchi Sea shelf (in blue) and the slope and western Arctic Ocean basin (in green).

of lower latitudes (62–68° N). Although the specific source of HBI-III in Arctic Ocean sediments has not been identified unequivocally, high pelagic HBI-III values in the IFZ and MIZ (Fig. 10c) are in agreement with the only known producer marine diatoms of the genera *Rhizosolenia* and *Pleurosigma* living at the sea-ice edge or in ice-free waters (Belt et al., 2017; Belt, 2018; Koch et al., 2020a; Smik et al., 2016). Consistent with our results, enhanced HBI-III has also been reported in surface sediments of the Barents Sea underlying the minimum and maximum April sea-ice margin (Belt et al., 2015). Further evidence was provided by sediment trap time series showing peaking HBI-III export flux at low sea ice and/or sea-ice retreat at the station in the Chukchi Sea slope (Bai et al., 2019; Gal et al., 2022). Dominant pelagic production in the northern Bering Sea is consistent with expanded open water areas and a lengthened phytoplankton growing season compared to more northern locations. Sea-ice thinning and melting are key factors responsible for increased primary production and northward expansion of phytoplankton blooms over the past decades (Renaut et al., 2018). Physical modeling also evidenced a clear northward shift of phytoplankton blooms from the Bering Sea to the Arctic shelf in the western Arctic Ocean with decreasing sea ice (Jin et al., 2012). Kahru et al. (2016) estimated an increase by 47 % of the net primary production across the Arctic Ocean between 1998 and 2015 in the spring and summer. These changes are largely due to enhanced incoming light resulting from earlier ice breakup in summer, later freezing in winter, increased open-water areas and a longer ice-free season boosting the phytoplankton production. In some areas, spring blooms along the sea-ice edge contribute more than half of the annual primary production and fall bloom becomes more

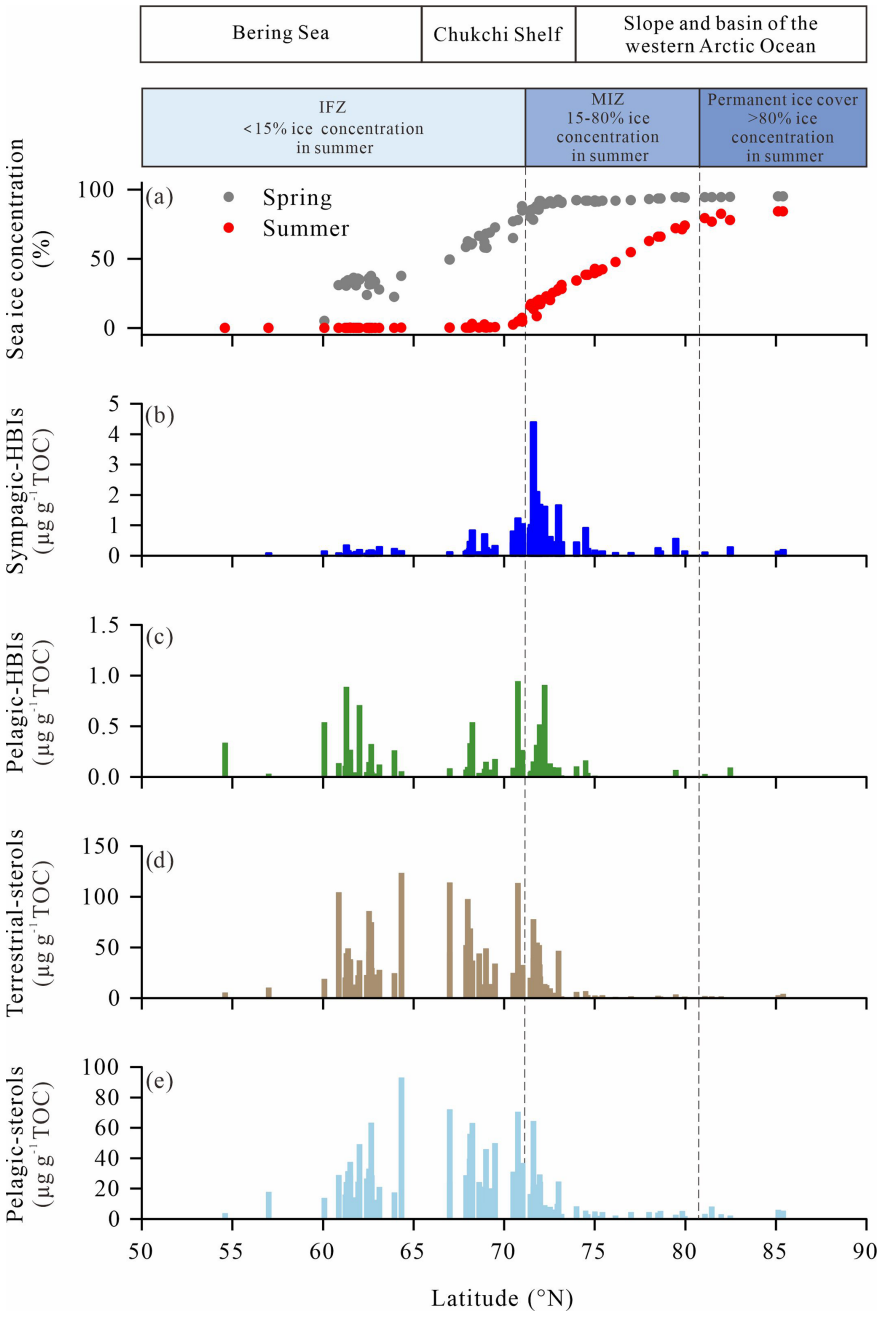

Figure 10. Concentrations of **(a)** spring and summer sea ice (in %) for the period 1994–2014 retrieved from NSIDC, **(b)** sympagic HBIs (IP_{25}, in $\mu g\,g^{-1}$ TOC), **(c)** pelagic HBIs (HBI-III, in $\mu g\,g^{-1}$ TOC), **(d)** terrestrial sterol (campesterol, in $\mu g\,g^{-1}$ TOC), **(e)** pelagic sterol (brassicasterol+dinosterol, in $\mu g\,g^{-1}$ TOC) in surface sediments along the latitudinal transect from the Bering Sea to the western Arctic Ocean.

frequent at latitudes $> 70°$ N (Ardyna et al., 2014). Other dynamical factors linked to the decline of sea ice can contribute to increased primary production such as wind-driven mixing and upwelling, both leading to the replenishment of surface waters with nutrients in the Chukchi Sea continental shelf (Huntington et al., 2020; Pickart et al., 2011). However, freshening associated with sea-ice melting and subsequent ocean stratification counteracts these processes by reducing nutrient availability in surface waters in summer–early fall. Finally, the PW represents a major source of nutrients for phytoplankton growth across the Bering Strait and along the coast of Alaska, which also allows for the intrusion of temperate species in the Arctic Ocean (Ardyna and Arrigo, 2020).

Pelagic phytosterols (e.g., brassicasterol and dinosterol) along our latitudinal gradient share a strong resemblance to HBI-III but show higher values relative to HBI-III in the IFZ, e.g., in the southern Chukchi shelf between 68 and 70° N (Fig. 10c–e). At latitudes > 81° N, on the slope and western Arctic basin under perennial sea ice, pelagic phytosterols drop to their lowest levels as a result of light and nutrient limitation (Fernández-Méndez et al., 2015; Gosselin et al., 1997). This result suggests that diatom production below sea ice is not significant at these extreme latitudes probably because of sea-ice thickness preventing light transmission, as also revealed by the OC and TN contents of the sediments (Arrigo et al., 2012, Coupel et al., 2012).

Interestingly, campesterol displays broadly similar features to phytosterols, with higher values found across the Bering Strait, at the northern Bering Sea and on the mid-Chukchi Sea shelf (Fig. 10d). The occurrence of branched and isoprenoid tetraethers in surface sediments in the Bering Sea and inner shelf of the Chukchi Sea (66–73° N) (Park et al., 2014) as well as $\delta^{13}C$ values < -25 ‰ (Grebmeier et al., 2006; Ji et al., 2019; Naidu et al., 2004) lends further support to a higher contribution of land-derived inputs to the sediments that is also reflected by our C/N values (Fig. 11c, d). Using the branch and isoprenoid tetraether (BIT) index as a proxy of terrestrial carbon, Park et al. (2014) reported low values on the outer shelf of the Chukchi Sea (73–75° N), moderate values offshore of the Bering Sea, inner shelf of the Chukchi Sea (66–73° N) and western Arctic Ocean north of 75° N, and the highest values in the Yukon and Mackenzie River estuaries. With the loss of continental ice and with increasing temperature and precipitation, enhanced biomass production on land and intensified erosion have resulted in increased river discharge of suspended particulate matter in the coastal Arctic Ocean. Changes in sea-ice distribution also influence terrestrial inputs to the sediment, through ice drifting from coastal areas (Darby et al., 2009; Eicken et al., 2005). Note that higher plant *n*-alkanes (Fig. 6) show no latitudinal trend and unexpectedly high values in the high Arctic, which demonstrate that allochthonous material reaches the central Arctic Ocean. The northwest Bering Sea higher values might be contributed by the Yukon River (Brabets et al., 2000), while high values in the southeastern Chukchi Sea shelf might be contributed by near-shore sea-ice transport, which bring massive black sediments when they form in the near shore close to Barrow Canyon (Darby et al., 2009; Harper, 1978).

5.3 Comparison of sterols in suspended particles with surface sediments

Biogeochemical data for the water column escape satellite measurements and are thus very scarce and critically needed to fully understand the impact of ongoing changes on primary production and the export and sequestration of organic carbon in the Arctic Ocean. As discussed in the previous sections, surface water properties are very sensitive to environmental changes linked to sea ice, which exerts a strong control on primary producers and ultimately on food resources (Lannuzel et al., 2020). The amount of exported organic material to the deep ocean depends on the structure of the phytoplankton community and subsequent higher trophic levels (Leu et al., 2011). The mismatch of spring phytoplankton bloom and zooplankton grazing activity caused by earlier sea-ice melting and earlier blooming could lead to a lower consumption of phytoplankton by grazing heterotrophs in the water column thereby also affecting export (Hunt et al., 2002; Søreide et al., 2010). In this section we investigate the sterols in suspended particles and underlying surface sediments in order to assess vertical transport pathways, although on a limited sample set.

As outlined earlier, higher contents of brassicasterol and dinosterol are localized in surface sediments of the Bering Sea shelf and the southeastern Chukchi Sea shelf and decrease sharply around 73° N to the north with increasing sea-ice cover (Fig. 11a, b). Despite the limited SPM sample set, brassicasterol and dinosterol in SPM reproduce the northward decrease with increasing sea ice similar to Chl *a*, with the highest values found in the south of the Chukchi Sea shelf (Fig. 7). The correlation between 24-ethylcholest-5-en-3β-ol and Chl *a* is significant ($r^2 = 0.90$, $p < 0.05$) (Fig. S2) and remains high even after the removal of the most extreme value ($r^2 = 0.79$, $p < 0.01$) (Fig. S3) pointing to a prevailing contribution of the marine-origin α isomer 24(α)-ethylcholest-5-en-3β-ol over the β isomer, β-sitosterol, as reported by Tolosa et al. (2013), who demonstrated the prevalence of 24(α)-ethylcholest-5-en-3β-ol even in coastal waters of the southeast Beaufort Sea. These observations are also in line with minor amounts below the detection limit of terrestrial biomarkers, e.g., campesterol and *n*-alkanes in SPM.

Cholesterol is usually a dominant sterol in zooplankton (Volkman, 1986) and has often been considered as an indicator of zooplankton activity (Grice et al., 1998), although this compound can also be produced by some algal species. Higher cholesterol abundances were essentially found in northern Bering Sea sediments (Fig. 11e). In suspended particles, linear regression led to correlation coefficients (r^2) of 0.99 and 0.79 (both $p > 0.05$) for cholesterol against brassicasterol and for cholesterol against dinosterol (Fig. S4). By contrast, for sediments, the statistical relationships between cholesterol and brassicasterol or cholesterol and dinosterol ($r^2 = 0.37$, $p < 0.01$ and $r^2 = 0.27$, $p < 0.01$, respectively; Fig. S5) are weak. Yet, phytoplankton and zooplankton living below sea ice and in the subsurface chlorophyll maximum, e.g., deeper than 5 m (our sampling depth), are not accounted for in the SPM, while they may represent an important component of primary production and exported material to the sea floor (Arrigo et al., 2012; Coupel et al., 2012). The timing of phytoplankton bloom and zooplankton grazing is another factor that could account for this discrepancy.

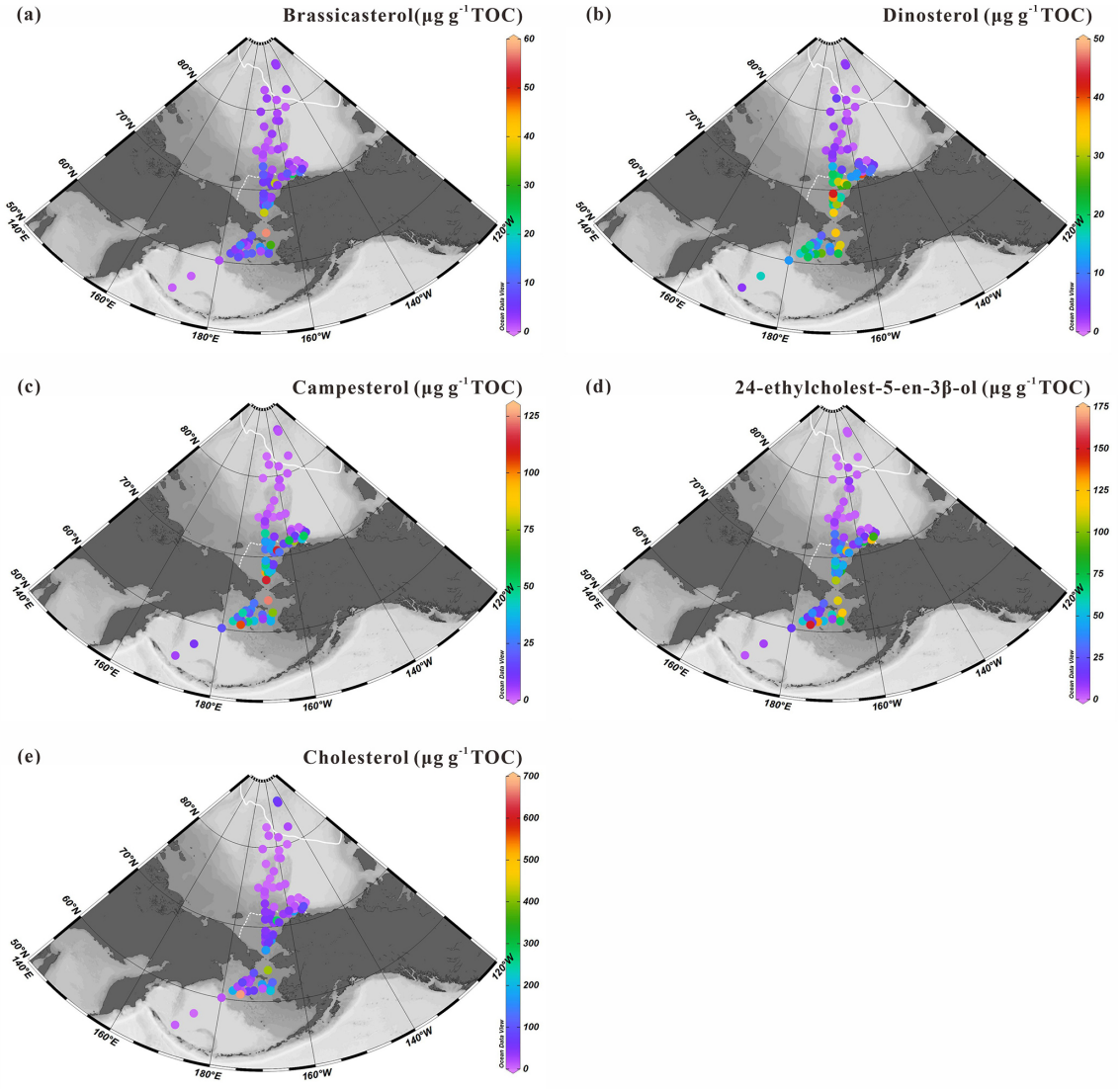

Figure 11. Concentrations of sterols normalized to TOC in surface sediments (expressed in $\mu g\,g^{-1}$ TOC): **(a)** brassicasterol and **(b)** dinosterol; **(c)** campesterol and **(d)** 24-ethylcholest-5-en-3β-ol; **(e)** cholesterol in the surface sediments ($n = 88$) from the western Arctic Ocean, the Chukchi Sea and the Bering Sea. For an explanation of the dotted and solid white lines, see Fig. 2.

Figure 12 shows the cholesterol and phytosterol concentrations in SPM and underlying surface sediments along a latitudinal transect between 69 and 79° N latitude. Sterols and Chl *a* both exhibit large-amplitude change in surface waters and underlying surface sediments from north to south. The highest brassicasterol and Chl *a* in surface waters of the northern Chukchi shelf at station 14R07 reflect the highly productive waters, underlined earlier in the Discussion, with a major contribution of diatom pigment fucoxanthin (Fig. 12a, b, Table S1). Zhuang et al. (2020) reported high biomass of diatoms ($> 20\,\mu m$) dominating in the subsurface chlorophyll maximum during the same cruise in summer 2014, south and north of the Chukchi shelf. This hotspot of primary production is sustained by continuous nutrient supply by the PW both during the ice-melting season and the ice-free season. The second highest Chl *a* and brassicasterol values of the transect are found at the southern site 14R03 bathed by low-nutrient ACW indicating the dominance of small diatoms ($< 20\,\mu m$) (Zhuang et al., 2020). To the north beyond the shelf, in the Chukchi slope and basin, SPM and sediments display the lowest Chl *a* and sterol values but show that primary production is still significant beyond the continental shelf. Similarly, Gosselin et al. (1997) reported that both phytoplankton and ice algal production were highest over the Chukchi shelf (70–72° N) and decreased poleward with increasing sea-ice cover and/or the depth of the surface mixed layer, both determining the light and nutrients available to microalgae growth. Arrigo et al. (2012) found

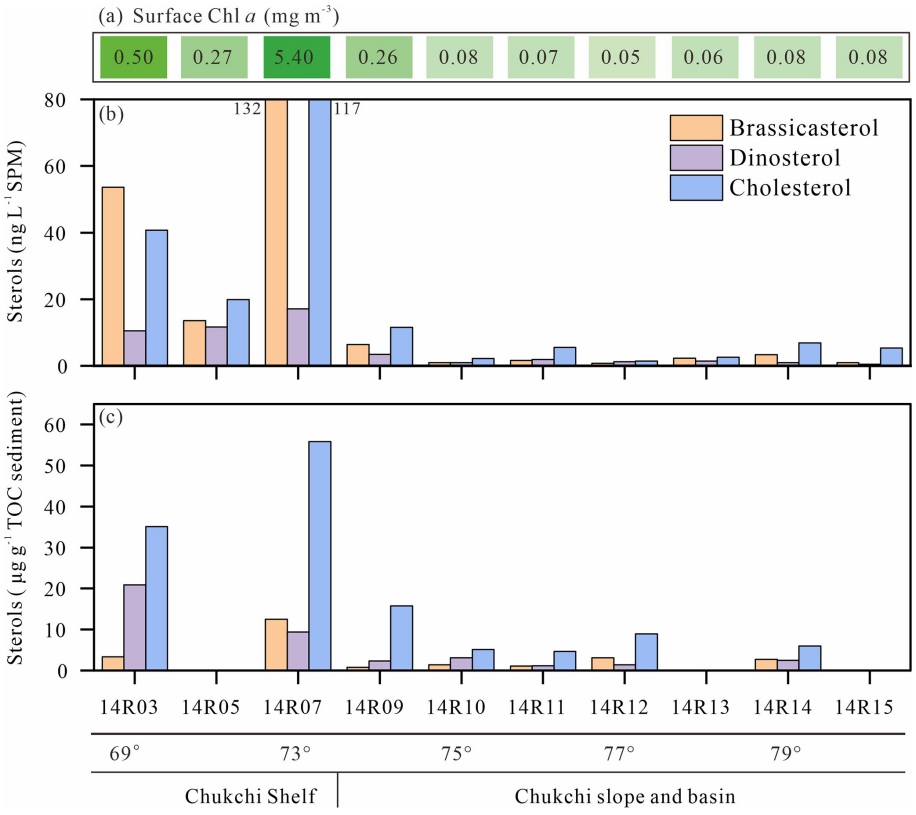

Figure 12. Concentrations in surface waters of Chl *a* **(a)**, brassicasterol, dinosterol and cholesterol in SPM **(b)**, and underlying surface sediments **(c)** along the transect from the shelf to the basin in the Chukchi Sea. For the location of the transect, see Fig. 7. Please note that there is no sediment sample at 14R05, 14R13 and 14R15.

Table 1. Ratios calculated from individual sterol concentrations in suspended particulate matter (SPM) and sediments from the Chukchi shelf and slope and the basin of the western Arctic Ocean.

	14R03	14R05	14R07	14R09	14R10	14R11	14R12	14R13	14R14	14R15
SPM										
B/C	1.32	0.68	1.13	0.55	0.42	0.30	0.54	0.86	0.48	0.19
D/C	0.26	0.59	0.15	0.30	0.42	0.34	0.84	0.55	0.14	0.09
B/D	5.10	1.16	7.73	1.84	1.01	0.89	0.65	1.55	3.51	1.95
Sediment										
B/C	0.10	–	0.22	0.05	0.27	0.23	0.35	–	0.45	–
D/C	0.60	–	0.17	0.15	0.60	0.24	0.15	–	0.41	–
B/D	0.16	–	1.34	0.32	0.44	0.94	2.26	–	1.11	–

Sterol: (B) brassicasterol (24-methylcholesta-5,22E-dien-3β-ol), (C) cholesterol (cholest-5-en-3β-ol), (D) dinosterol (4α, 23, 24R-trimethyl-5α-cholest-22E-en-3β-ol).

massive under-ice phytoplankton bloom over the Chukchi shelf around 73° N, supported by light transmission through first-year ice (0.8–1.3 m in thickness) due to thinning sea ice and proliferation of melt ponds. Dominating brassicasterol over dinosterol in surface SPM in the Chukchi shelf (stations 14R03, 14R05 and 14R07) indicates diatom-rich waters in the MIZ (Table 1). However, underlying sediments evidence limited export of brassicasterol compared to dinosterol, suggesting efficient grazing of diatoms and their transfer in the food web. At the southernmost station 14R03, phytoplankton in surface waters was dominated by small diatoms that are more inclined to remain and degrade in the upper layer, because they can hardly sink if not grazed (Table S1). Another explanation for the different vertical transport is that 14R03

experienced ice-free and stratified conditions in summer that favor the development of dinoflagellates late in the season and their more efficient export to surface sediments while diatoms seem to be mostly consumed early in the spring bloom season. High cholesterol abundances in the mid-Chukchi Sea shelf SPM and underlying sediments reflect the consumption by herbivorous zooplankton and export through fecal pellets in the richest phytoplankton waters (Fig. 12b, c). It also underlines the preservation of organic matter in shallow sediments of the Chukchi shelf. With the exception of site 14R05, for which sediment data are missing, these finding are illustrated by brassicasterol/cholesterol ratios (B/C) mainly > 1 and are highly variable in the SPM over the Chukchi shelf, and $B/C < 1$ in the Chukchi slope and basin (Table 1). Prevailing cholesterol in surface sediments associated with $B/C < 1$ and $D/C < 1$ further emphasizes the role of zooplankton and grazing pressure on primary producers in the rich waters of the MIZ and the likely efficient transfer to higher trophic levels.

6 Conclusions

Using the HBI biomarkers and H-Print sea-ice index of 88 surface sediments distributed along a latitudinal transect from the Bering Sea to the high Arctic, we were able to distinguish three biogeographic regions: (i) the Bering Sea exhibiting a high variability of enhanced pelagic-to-sympagic production reflecting a wide range of sea-ice conditions of the IFZ more strongly influenced by the PDO than global warming, (ii) the mid-Chukchi Sea shelf productive waters characterized by higher and less variable sympagic production due to variable sea-ice conditions of the MIZ, and (iii) the slope and western Arctic Ocean basin displaying higher sympagic relative to pelagic production constrained by a higher sea-ice cover and narrow variability. Our results also underline the role of PW inflow in shaping local environmental changes and primary production in the mid-Chukchi Sea shelf located in the MIZ through heat and nutrient transport.

Our data evidence a conspicuous latitudinal trend in phytoplankton population with increasing sympagic relative to pelagic production northward and the highest production and export of both sea-ice microalgae and pelagic diatoms in the MIZ in the mid-Chukchi continental shelf. Low terrestrial sterols and *n*-alkanes in surface sediments underscore a low terrigenous contribution to the sediments with no clear latitudinal trend, highlighting different sources and transport pathways than marine organic matter. This is further confirmed by their absence or being below detection level in suspended particles between 68.6 and 79.4° N. Quite unusually, we also found that the 24-ethylcholest-5-en-3β-ol was essentially represented by the marine α-isomer, the 24(α)-ethylcholest-5-en-3β-ol, even at most coastal sites.

Comparisons of phytosterol and cholesterol fingerprints between SPM and surface sediments suggest the efficient consumption of ice microalgae and pelagic diatoms during the spring blooms as compared to dinoflagellates that generally thrive under stratified conditions toward the end of the production season. However, more investigations in the water column and of the sinking particle flux are needed for a comprehensive picture of the fate and behavior of phyto- and zooplankton. An integrated approach combining trophic biomarkers such as fatty acids and carbon stable isotopes could serve as a basis to explore further the links between phyto- and zooplankton in this complex environment and improve our understanding of the fate of sea-ice algae and pelagic production and their dynamics across the food web. This knowledge is essential for evaluating the future evolution of marine resources for local populations as well as for assessing the amount of OC transferred and sequestered to the sea floor in order to also advance our understanding of carbon cycle feedback mechanisms on climate in this rapidly changing Pacific Arctic system.

Data availability. All data that support the findings of this study are included with the article (and Supplement files).

Supplement. The supplement related to this article is available online at: https://doi.org/10.5194/bg-21-689-2024-supplement.

Author contributions. YB and JC designed the study. MAS initiated the writing of the paper with YB and JR. VK contributed the biomarker analyses (HBIs and sterols) and paper content. HJ acquired funding from the Chinese Arctic and Antarctic Administration and made edits to the final version.

Competing interests. The contact author has declared that none of the authors has any competing interests.

Disclaimer. Publisher's note: Copernicus Publications remains neutral with regard to jurisdictional claims made in the text, published maps, institutional affiliations, or any other geographical representation in this paper. While Copernicus Publications makes every effort to include appropriate place names, the final responsibility lies with the authors.

Acknowledgements. We are grateful to the captain, crew members and scientific team of the R/V *Xuelong* for their help with the retrieval of the surface water suspended particulate matter and surface sediments. We also thank Fanny Kaczmar, who helped produce HBI data at LOCEAN, and to Guillaume Massé for supplying chemical standards for HBI quantification. We thank the Centre National de la Recherche Scientifique (CNRS) for salary support of Marie-Alexandrine Sicre and Vincent Klein and for biomarker analyses.

We thank Zhongqiang Ji, Liang Su and Yang Zhang for TOC and TN determinations of surface sediments, Hongliang Li and Yanpei Zhuang for sediment sampling and Qiang Hao for Chl *a* analyses in the surface water. We also thank Xiaotong Xiao and Long Lin for assistance in retrieving sea-ice concentration data. The pigment data used in this work are available from the Data-Sharing Platform of Polar Science (https://datacenter.chinare.org.cn/, last access: 25 July 2023) maintained by the Chinese National Arctic & Antarctic Data Center (CN-NADC).

Financial support. This study was funded by the National Key Research and Development Program of China (No. 2019YFE0120900), the National Natural Science Foundation of China (Nos. 41976229, 41941013, 41776205, 42076241 and 42376243), the Scientific Research Funds of the Second Institute of Oceanography, MNR (No. JG2310), the Chinese Polar Environmental Comprehensive Investigation and Assessment Programs (No. CHINARE 0304), and the project ICAR (Sea Ice melt, Carbon, Acidification and Phytoplankton in the present and past Arctic Ocean) funded by the Cai Yuan Pei Program.

Review statement. This paper was edited by Sebastian Naeher and reviewed by two anonymous referees.

References

Ardyna, M. and Arrigo, K. R.: Phytoplankton dynamics in a changing Arctic Ocean, Nat. Clim. Change, 10, 892–903, https://doi.org/10.1038/s41558-020-0905-y, 2020.

Ardyna, M., Babin, M., Gosselin, M., Devred, E., Rainville, L., and Tremblay, J.-É.: Recent Arctic Ocean sea ice loss triggers novel fall phytoplankton blooms, Geophys. Res. Lett., 41, 6207–6212, https://doi.org/10.1002/2014GL061047, 2014.

Ardyna, M., Mundy, C. J., Mayot, N., Matthes, L. C., Oziel, L., Horvat, C., Leu, E., Assmy, P., Hill, V., Matrai, P. A., Gale, M., Melnikov, I. A., and Arrigo, K. R.: Under-Ice Phytoplankton Blooms: Shedding Light on the "Invisible" Part of Arctic Primary Production, Front. Mar. Sci., 7, 608032, https://doi.org/10.3389/fmars.2020.608032, 2020.

Arrigo, K. R. and van Dijken, G. L.: Secular trends in Arctic Ocean net primary production, J. Geophys. Res.-Oceans, 116, https://doi.org/10.1029/2011JC007151, 2011.

Arrigo, K. R., Perovich, D. K., Pickart, R. S., Brown, Z. W., van Dijken, G. L., Lowry, K. E., Mills, M. M., Palmer, M. A., Balch, W. M., Bahr, F., Bates, N. R., Benitez-Nelson, C., Bowler, B., Brownlee, E., Ehn, J. K., Frey, K. E., Garley, R., Laney, S. R., Lubelczyk, L., Mathis, J., Matsuoka, A., Mitchell, B. G., Moore, G. W. K., Ortega-Retuerta, E., Pal, S., Polashenski, C. M., Reynolds, R. A., Schieber, B., Sosik, H. M., Stephens, M., and Swift, J. H.: Massive Phytoplankton Blooms Under Arctic Sea Ice, Science, 336, 1408–1408, https://doi.org/10.1126/science.1215065, 2012.

Arrigo, K. R.: Sea ice as a habitat for primary producers, in: Sea Ice, 352–369, https://doi.org/10.1002/9781118778371.ch14, 2017.

Bai, Y., Sicre, M.-A., Chen, J., Klein, V., Jin, H., Ren, J., Li, H., Xue, B., Ji, Z., Zhuang, Y., and Zhao, M.: Seasonal and spatial variability of sea ice and phytoplankton biomarker flux in the Chukchi sea (western Arctic Ocean), Prog. Oceanogr., 171, 22–37, https://doi.org/10.1016/j.pocean.2018.12.002, 2019.

Belt, S. T. and Müller, J.: The Arctic sea ice biomarker IP25: a review of current understanding, recommendations for future research and applications in palaeo sea ice reconstructions, Quat. Sci. Rev., 79, 9–25, https://doi.org/10.1016/j.quascirev.2012.12.001, 2013.

Belt, S. T., Brown, T. A., Smik, L., Tatarek, A., Wiktor, J., Stowasser, G., Assmy, P., Allen, C. S., and Husum, K.: Identification of C25 highly branched isoprenoid (HBI) alkenes in diatoms of the genus Rhizosolenia in polar and subpolar marine phytoplankton, Organ. Geochem.,, 110, 65–72, https://doi.org/10.1016/j.orggeochem.2017.05.007, 2017.

Belt, S. T., Cabedo-Sanz, P., Smik, L., Navarro-Rodriguez, A., Berben, S. M. P., Knies, J., and Husum, K.: Identification of paleo Arctic winter sea ice limits and the marginal ice zone: Optimised biomarker-based reconstructions of late Quaternary Arctic sea ice, Earth Planet. Sc. Lett., 431, 127–139, https://doi.org/10.1016/j.epsl.2015.09.020, 2015.

Belt, S. T., Massé, G., Rowland, S. J., Poulin, M., Michel, C., and LeBlanc, B.: A novel chemical fossil of palaeo sea ice: IP25, Organ. Geochem., 38, 16–27, https://doi.org/10.1016/j.orggeochem.2006.09.013, 2007.

Belt, S. T.: Source-specific biomarkers as proxies for Arctic and Antarctic sea ice, Organ. Geochem., 125, 277–298, https://doi.org/10.1016/j.orggeochem.2018.10.002, 2018.

Boetius, A., Albrecht, S., Bakker, K., Bienhold, C., Felden, J., Fernández-Méndez, M., Hendricks, S., Katlein, C., Lalande, C., Krumpen, T., Nicolaus, M., Peeken, I., Rabe, B., Rogacheva, A., Rybakova, E., Somavilla, R., Wenzhöfer, F., and RV *Polarstern* ARK 27-3-S.S. Party: Export of Algal Biomass from the Melting Arctic Sea Ice, Science, 339, 1430–1432, https://doi.org/10.1126/science.1231346, 2013.

Brabets, T. P., Wang, B., Meade, R. H.: Environmental and hydrologic overview of the Yukon River Basin, Alaska and Canada, U.S. Geological Survey Water-Resources Investigations Report, 106 pp., 2000.

Brown, K. A., Holding, J. M., and Carmack, E. C.: Understanding Regional and Seasonal Variability Is Key to Gaining a Pan-Arctic Perspective on Arctic Ocean Freshening, Front. Mar. Sci., 7, 606, https://doi.org/10.3389/fmars.2020.00606, 2020.

Brown, T. A., Belt, S. T., Philippe, B., Mundy, C. J., Massé, G., Poulin, M., and Gosselin, M.: Temporal and vertical variations of lipid biomarkers during a bottom ice diatom bloom in the Canadian Beaufort Sea: further evidence for the use of the IP25 biomarker as a proxy for spring Arctic sea ice, Polar Biol., 34, 1857–1868, https://doi.org/10.1007/s00300-010-0942-5, 2011.

Brown, T. A., Belt, S. T., Tatarek, A., and Mundy, C. J.: Source identification of the Arctic sea ice proxy IP25, Nat. Commun., 5, 4197, https://doi.org/10.1038/ncomms5197, 2014a.

Brown, T. A., Yurkowski, D. J., Ferguson, S. H., Alexander, C., and Belt, S. T.: H-Print: a new chemical fingerprinting approach for distinguishing primary production sources in Arctic ecosystems, Environ. Chem. Lett., 12, 387–392, https://doi.org/10.1007/s10311-014-0459-1, 2014b.

Cautain, I. J., Last, K. S., McKee, D., Bluhm, B. A., Renaud, P. E., Ziegler, A. F., and Narayanaswamy, B. E.: Uptake of sympagic organic carbon by the Barents Sea benthos

linked to sea ice seasonality, Front. Mar. Sci., 9, 1009303, https://doi.org/10.3389/fmars.2022.1009303, 2022.

Coachman, L. K., Aagaard, K., and Tripp, R. B.: Bering Strait: the regional physical oceanography, University of Washington Press, 72 pp., 1975.

Coupel, P., Jin, H. Y., Joo, M., Horner, R., Bouvet, H. A., Sicre, M.-A., Gascard, J.-C., Chen, J. F., Garçon, V., and Ruiz-Pino, D.: Phytoplankton distribution in unusually low sea ice cover over the Pacific Arctic, Biogeosciences, 9, 4835–4850, https://doi.org/10.5194/bg-9-4835-2012, 2012.

Coupel, P., Ruiz-Pino, D., Sicre, M. A., Chen, J. F., Lee, S. H., Schiffrine, N., Li, H. L., and Gascard, J. C.: The impact of freshening on phytoplankton production in the Pacific Arctic Ocean, Prog. Oceanogr., 131, 113–125, https://doi.org/10.1016/j.pocean.2014.12.003, 2015.

Darby, D. A., Ortiz, J., Polyak, L., Lund, S., Jakobsson, M., and Woodgate, R. A.: The role of currents and sea ice in both slowly deposited central Arctic and rapidly deposited Chukchi–Alaskan margin sediments, Global Planet. Change, 68, 58–72, https://doi.org/10.1016/j.gloplacha.2009.02.007, 2009.

DiGirolamo, N. E., Parkinson, C. L., Cavalieri, D. J., Gloersen, P., and Zwally, H. J.: Sea Ice Concentrations from Nimbus-7 SMMR and DMSP SSM/I-SSMIS Passive Microwave Data, Version 2 [Data Set], Boulder, Colorado USA. NASA National Snow and Ice Data Center Distributed Active Archive Center, https://doi.org/10.5067/MPYG15WAA4WX, 2022.

Ehrlich, J., Bluhm, B. A., Peeken, I., Massicotte, P., Schaafsma, F. L., Castellani, G., Brandt, A., and Flores, H.: Sea-ice associated carbon flux in Arctic spring, Elementa, 9, 00169, https://doi.org/10.1525/elementa.2020.00169, 2021.

Eicken, H., Gradinger, R., Gaylord, A., Mahoney, A., Rigor, I., and Melling, H.: Sediment transport by sea ice in the Chukchi and Beaufort Seas: Increasing importance due to changing ice conditions?, Deep Sea Res. Pt. II, 52, 3281–3302, 2005.

Fahl, K. and Stein, R.: Biomarkers as organic-carbon-source and environmental indicators in the Late Quaternary Arctic Ocean: problems and perspectives, Mar. Chem., 63, 293–309, https://doi.org/10.1016/S0304-4203(98)00068-1, 1999.

Fernández-Méndez, M., Katlein, C., Rabe, B., Nicolaus, M., Peeken, I., Bakker, K., Flores, H., and Boetius, A.: Photosynthetic production in the central Arctic Ocean during the record sea-ice minimum in 2012, Biogeosciences, 12, 3525–3549, https://doi.org/10.5194/bg-12-3525-2015, 2015.

Gal, J.-K., Ha, S.-Y., Park, J., Shin, K.-H., Kim, D., Kim, N.-Y., Kang, S.-H., and Yang, E. J.: Seasonal Flux of Ice-Related Organic Matter During Under-Ice Blooms in the Western Arctic Ocean Revealed by Algal Lipid Biomarkers, J. Geophys. Res.-Oceans, 127, e2021JC017914, https://doi.org/10.1029/2021JC017914, 2022.

Gosselin, M., Levasseur, M., Wheeler, P. A., Horner, R. A., and Booth, B. C.: New measurements of phytoplankton and ice algal production in the Arctic Ocean, Deep Sea Res. Pt. II, 44, 1623–1644, https://doi.org/10.1016/S0967-0645(97)00054-4, 1997.

Gradinger, R.: Sea-ice algae: Major contributors to primary production and algal biomass in the Chukchi and Beaufort Seas during May/June 2002, Deep Sea Res. Pt. II, 56, 1201–1212, https://doi.org/10.1016/j.dsr2.2008.10.016, 2009.

Gradinger, R.: Vertical fine structure of the biomass and composition of algal communities in Arctic pack ice, Mar. Biol., 133, 745–754, https://doi.org/10.1007/s002270050516, 1999.

Grebmeier, J. M., Cooper, L. W., Feder, H. M., and Sirenko, B. I.: Ecosystem dynamics of the Pacific-influenced Northern Bering and Chukchi Seas in the Amerasian Arctic, Prog. Oceanogr., 71, 331–361, https://doi.org/10.1016/j.pocean.2006.10.001, 2006.

Grebmeier, J. M., McRoy, C. P., and Feder, H. M.: Pelagic-benthic coupling on the shelf of the northern Bering and Chukchi Seas, I. Food supply source and benthic biomass, Mar. Ecol. Prog. Ser., 48, 57–67, 1988.

Grice, K., Klein Breteler, W. C. M., Schouten, S., Grossi, V., de Leeuw, J. W., and Damsté, J. S. S.: Effects of zooplankton herbivory on biomarker proxy records, Paleoceanography, 13, 686–693, https://doi.org/10.1029/98PA01871, 1998.

Harada, N.: Review: Potential catastrophic reduction of sea ice in the western Arctic Ocean: Its impact on biogeochemical cycles and marine ecosystems, Global Planet. Change, 136, 1–17, https://doi.org/10.1016/j.gloplacha.2015.11.005, 2016.

Harper, J. R.: Coastal Erosion Rates along the Chukchi Sea Coast Near Barrow, Alaska, Arctic, 31, 428–433, 1978.

Hill, V., Ardyna, M., Lee, S. H., and Varela, D. E.: Decadal trends in phytoplankton production in the Pacific Arctic Region from 1950 to 2012, Deep Sea Res. Pt. II, 152, 82–94, https://doi.org/10.1016/j.dsr2.2016.12.015, 2018.

Holm-Hansen, O., Lorenzen, C. J., Holmes, R. W., and Strickland, J. D. H.: Fluorometric Determination of Chlorophyll, ICES J. Mar. Sci., 30, 3–15, https://doi.org/10.1093/icesjms/30.1.3, 1965.

Hop, H., Vihtakari, M., Bluhm, B. A., Assmy, P., Poulin, M., Gradinger, R., Peeken, I., von Quillfeldt, C., Olsen, L. M., Zhitina, L., and Melnikov, I. A.: Changes in Sea-Ice Protist Diversity With Declining Sea Ice in the Arctic Ocean From the 1980s to 2010s, Front. Mar. Sci., 7, 243, https://doi.org/10.3389/fmars.2020.00243, 2020.

Hunt Jr, G. L., Stabeno, P., Walters, G., Sinclair, E., Brodeur, R. D., Napp, J. M., and Bond, N. A.: Climate change and control of the southeastern Bering Sea pelagic ecosystem, Deep Sea Res. Pt. II, 49, 5821–5853, https://doi.org/10.1016/S0967-0645(02)00321-1, 2002.

Hunt, G. L., Blanchard, A. L., Boveng, P., Dalpadado, P., Drinkwater, K. F., Eisner, L., Hopcroft, R. R., Kovacs, K. M., Norcross, B. L., Renaud, P., Reigstad, M., Renner, M., Skjoldal, H. R., Whitehouse, A., and Woodgate, R. A.: The Barents and Chukchi Seas: Comparison of two Arctic shelf ecosystems, J. Mar. Syst., 109, 43–68, https://doi.org/10.1016/j.jmarsys.2012.08.003, 2013.

Huntington, H. P., Danielson, S. L., Wiese, F. K., Baker, M., Boveng, P., Citta, J. J., De Robertis, A., Dickson, D. M. S., Farley, E., George, J. C., Iken, K., Kimmel, D. G., Kuletz, K., Ladd, C., Levine, R., Quakenbush, L., Stabeno, P., Stafford, K. M., Stockwell, D., and Wilson, C.: Evidence suggests potential transformation of the Pacific Arctic ecosystem is underway, Nat. Clim. Change, 10, 342–348, https://doi.org/10.1038/s41558-020-0695-2, 2020.

Jakobsson, M., Andreassen, K., Bjarnadóttir, L. R., Dove, D., Dowdeswell, J. A., England, J. H., Funder, S., Hogan, K., Ingólfsson, Ó., Jennings, A., Krog Larsen, N., Kirchner, N., Landvik, J. Y., Mayer, L., Mikkelsen, N., Möller, P., Niessen, F., Nilsson, J., O'Regan, M., Polyak, L., Nørgaard-Pedersen, N., and

Stein, R.: Arctic Ocean glacial history, Quat. Sci. Rev., 92, 40–67, https://doi.org/10.1016/j.quascirev.2013.07.033, 2014.

Ji, R., Ashjian, C. J., Campbell, R. G., Chen, C., Gao, G., Davis, C. S., Cowles, G. W., and Beardsley, R. C.: Life history and biogeography of Calanus copepods in the Arctic Ocean: An individual-based modeling study, Prog. Oceanogr., 96, 40–56, https://doi.org/10.1016/j.pocean.2011.10.001, 2012.

Ji, Z., Jin, H., Stein, R., Li, Z., Bai, Y., Li, H., Zhang, Y., and Chen, J.: Distribution and Sources of Organic Matter in Surface Sediments of the Northern Bering and Chukchi Seas by Using Bulk and Tetraether Proxies, J. Ocean Univ. China, 18, 563–572, https://doi.org/10.1007/s11802-019-3869-7, 2019.

Jin, M., Deal, C., Lee, S. H., Elliott, S., Hunke, E., Maltrud, M., and Jeffery, N.: Investigation of Arctic sea ice and ocean primary production for the period 1992–2007 using a 3-D global ice–ocean ecosystem model, Deep Sea Res. Pt. II, 81, 28–35, https://doi.org/10.1016/j.dsr2.2011.06.003, 2012.

Kahru, M., Lee, Z., Mitchell, B. G., and Nevison, C. D.: Effects of sea ice cover on satellite-detected primary production in the Arctic Ocean, Biol. Lett., 12, 20160223, https://doi.org/10.1098/rsbl.2016.0223, 2016.

Koch, C. W., Cooper, L. W., Lalande, C., Brown, T. A., Frey, K. E., and Grebmeier, J. M.: Seasonal and latitudinal variations in sea ice algae deposition in the Northern Bering and Chukchi Seas determined by algal biomarkers, PLOS ONE, 15, e0231178, https://doi.org/10.1371/journal.pone.0231178, 2020a.

Koch, C. W., Cooper, L. W., Grebmeier, J. M., Frey, K., and Brown, T. A.: Ice algae resource utilization by benthic macro- and megafaunal communities on the Pacific Arctic shelf determined through lipid biomarker analysis, Mar. Ecol. Prog. Ser., 651, 23–43, 2020b.

Koch, C. W., Brown, T. A., Amiraux, R., Ruiz-Gonzalez, C., MacCorquodale, M., Yunda-Guarin, G. A., Kohlbach, D., Loseto, L. L., Rosenberg, B., and Hussey, N. E.: Year-round utilization of sea ice-associated carbon in Arctic ecosystems, Nat. Commun., 14, 1964, https://doi.org/10.1038/s41467-023-37612-8, 2023.

Kohlbach, D., Graeve, M., A. Lange, B., David, C., Peeken, I., and Flores, H.: The importance of ice algae-produced carbon in the central Arctic Ocean ecosystem: Food web relationships revealed by lipid and stable isotope analyses, Limnol. Oceanogr., 61, 2027–2044, https://doi.org/10.1002/lno.10351, 2016.

Kolling, H. M., Stein, R., Fahl, K., Sadatzki, H., de Vernal, A., and Xiao, X.: Biomarker Distributions in (Sub)-Arctic Surface Sediments and Their Potential for Sea Ice Reconstructions, Geochem. Geophys. Geosyst., 21, e2019GC008629, https://doi.org/10.1029/2019GC008629, 2020.

Kolling, H., Schneider, R., Gross, F., Hamann, C., Kienast, M., Kienast, S., Doering, K., Fahl, K., and Stein, R.: Biomarker Records of Environmental Shifts on the Labrador Shelf During the Holocene, Paleoceanogr. Paleoclimatol., 38, e2022PA004578, https://doi.org/10.1029/2022PA004578, 2023.

Lannuzel, D., Tedesco, L., van Leeuwe, M., Campbell, K., Flores, H., Delille, B., Miller, L., Stefels, J., Assmy, P., Bowman, J., Brown, K., Castellani, G., Chierici, M., Crabeck, O., Damm, E., Else, B., Fransson, A., Fripiat, F., Geilfus, N.-X., Jacques, C., Jones, E., Kaartokallio, H., Kotovitch, M., Meiners, K., Moreau, S., Nomura, D., Peeken, I., Rintala, J.-M., Steiner, N., Tison, J.-L., Vancoppenolle, M., Van der Linden, F., Vichi, M., and Wongpan, P.: The future of Arctic sea-ice biogeochemistry and ice-associated ecosystems, Nat. Clim. Change, 10, 983–992, https://doi.org/10.1038/s41558-020-00940-4, 2020.

Legendre, L., Ackley, S. F., Dieckmann, G. S., Gulliksen, B., Horner, R., Hoshiai, T., Melnikov, I. A., Reeburgh, W. S., Spindler, M., and Sullivan, C. W.: Ecology of sea ice biota, Polar Biol., 12, 429–444, https://doi.org/10.1007/BF00243114, 1992.

Leu, E., Søreide, J. E., Hessen, D. O., Falk-Petersen, S., and Berge, J.: Consequences of changing sea-ice cover for primary and secondary producers in the European Arctic shelf seas: Timing, quantity, and quality, Prog. Oceanogr., 90, 18–32, https://doi.org/10.1016/j.pocean.2011.02.004, 2011.

Li, W. K., McLaughlin, F. A., Lovejoy, C., and Carmack, E. C.: Smallest algae thrive as the Arctic Ocean freshens, Science, 326, 539–539, 2009.

Massé, G., Rowland, S. J., Sicre, M.-A., Jacob, J., Jansen, E., and Belt, S. T.: Abrupt climate changes for Iceland during the last millennium: Evidence from high resolution sea ice reconstructions, Earth Planet. Sc. Lett., 269, 565–569, https://doi.org/10.1016/j.epsl.2008.03.017, 2008.

Masson-Delmotte, V., Zhai, P., Pirani, A., Connors, S. L., Péan, C., Berger, S., Caud, N., Chen, Y., Goldfarb, L., Gomis, M. I., Huang, M., Leitzell, K., Lonnoy, E., Matthews, J. B. R., Maycock, T. K., Waterfield, T., Yelekçi, O., Yu, R., and Zhou, B. (Eds.): IPCC, 2021: Climate Change 2021: The Physical Science Basis. Contribution of Working Group I to the Sixth Assessment Report of the Intergovernmental Panel on Climate Change, Cambridge University Press, United Kingdom and New York, NY, USA, https://doi.org/10.1017/9781009157896, 2021.

Méheust, M., Fahl, K., and Stein, R.: Variability in modern sea surface temperature, sea ice and terrigenous input in the sub-polar North Pacific and Bering Sea: Reconstruction from biomarker data, Organ. Geochem., 57, 54–64, https://doi.org/10.1016/j.orggeochem.2013.01.008, 2013.

Moore, S. E. and Grebmeier, J. M.: The Distributed Biological Observatory: Linking Physics to Biology in the Pacific Arctic Region, Arctic, 71, 1–7, 2018.

Moran, S. B., Lomas, M. W., Kelly, R. P., Gradinger, R., Iken, K., and Mathis, J. T.: Seasonal succession of net primary productivity, particulate organic carbon export, and autotrophic community composition in the eastern Bering Sea, Deep Sea Res. Pt. II, 65, 84–97, https://doi.org/10.1016/j.dsr2.2012.02.011, 2012.

Müller, J., Wagner, A., Fahl, K., Stein, R., Prange, M., and Lohmann, G.: Towards quantitative sea ice reconstructions in the northern North Atlantic: A combined biomarker and numerical modelling approach, Earth Planet. Sc. Lett., 306, 137–148, https://doi.org/10.1016/j.epsl.2011.04.011, 2011.

Naidu, A., Cooper, L., Grebmeier, J., Whitledge, T., and Hameedi, M.: The continental margin of the North Bering-Chukchi Sea: concentrations, sources, fluxes, accumulation and burial rates of organic carbon, The Organic Carbon Cycle in the Arctic Ocean, 193–203, 2004.

Park, Y.-H., Yamamoto, M., Nam, S.-I., Irino, T., Polyak, L., Harada, N., Nagashima, K., Khim, B.-K., Chikita, K., and Saitoh, S.-I.: Distribution, source and transportation of glycerol dialkyl glycerol tetraethers in surface sediments from the western Arctic Ocean and the northern Bering Sea, Mar. Chem., 165, 10–24, https://doi.org/10.1016/j.marchem.2014.07.001, 2014.

Park, J. H., Kim, S.-J., Lim, H.-G., Kug, J.-S., Yang, E. J., and Kim, B.-M.: Phytoplankton responses to increasing Arctic river

discharge under the present and future climate simulations, Environ. Res. Lett., 18, 064037, https://doi.org/10.1088/1748-9326/acd568, 2023.

Pearce, C., Varhelyi, A., Wastegård, S., Muschitiello, F., Barrientos, N., O'Regan, M., Cronin, T. M., Gemery, L., Semiletov, I., Backman, J., and Jakobsson, M.: The 3.6 ka Aniakchak tephra in the Arctic Ocean: a constraint on the Holocene radiocarbon reservoir age in the Chukchi Sea, Clim. Past, 13, 303–316, https://doi.org/10.5194/cp-13-303-2017, 2017.

Pickart, R. S., Spall, M. A., Moore, G. W. K., Weingartner, T. J., Woodgate, R. A., Aagaard, K., and Shimada, K.: Upwelling in the Alaskan Beaufort Sea: Atmospheric forcing and local versus non-local response, Prog. Oceanogr., 88, 78–100, https://doi.org/10.1016/j.pocean.2010.11.005, 2011.

Polyak, L., Bischof, J., Ortiz, J. D., Darby, D. A., Channell, J. E. T., Xuan, C., Kaufman, D. S., Løvlie, R., Schneider, D. A., Eberl, D. D., Adler, R. E., and Council, E. A.: Late Quaternary stratigraphy and sedimentation patterns in the western Arctic Ocean, Global Planet. Change, 68, 5–17, https://doi.org/10.1016/j.gloplacha.2009.03.014, 2009.

Renaut, S., Devred, E., and Babin, M.: Northward Expansion and Intensification of Phytoplankton Growth During the Early Ice-Free Season in Arctic, Geophys. Res. Lett., 45, 10590–10598, https://doi.org/10.1029/2018GL078995, 2018.

Roach, A. T., Aagaard, K., Pease, C. H., Salo, S. A., Weingartner, T., Pavlov, V., and Kulakov, M.: Direct measurements of transport and water properties through the Bering Strait, J. Geophys. Res.-Oceans, 100, 18443–18457, https://doi.org/10.1029/95JC01673, 1995.

Schlitzer, Reiner, Ocean Data View, https://odv.awi.de/ (last access: 14 November 2023), 2023.

Schmidt, K., Brown, T. A., Belt, S. T., Ireland, L. C., Taylor, K. W. R., Thorpe, S. E., Ward, P., and Atkinson, A.: Do pelagic grazers benefit from sea ice? Insights from the Antarctic sea ice proxy IPSO25, Biogeosciences, 15, 1987–2006, https://doi.org/10.5194/bg-15-1987-2018, 2018.

Shimada, K., Kamoshida, T., Itoh, M., Nishino, S., Carmack, E., McLaughlin, F., Zimmermann, S., and Proshutinsky, A.: Pacific Ocean inflow: Influence on catastrophic reduction of sea ice cover in the Arctic Ocean, Geophys. Res. Lett., 33, L08605, https://doi.org/10.1029/2005GL025624, 2006.

Smik, L., Cabedo-Sanz, P., and Belt, S. T.: Semi-quantitative estimates of paleo Arctic sea ice concentration based on source-specific highly branched isoprenoid alkenes: A further development of the PIP25 index, Organ. Geochem., 92, 63–69, https://doi.org/10.1016/j.orggeochem.2015.12.007, 201

Søreide,, J. E., Leu, E., Berge, J., Graeve, M., and Falk-Petersen, S.: Timing of blooms, algal food quality and Calanus glacialis reproduction and growth in a changing Arctic, Global Change Biology, 16, 3154–3163, https://doi.org/10.1111/j.1365-2486.2010.02175.x, 2010.

Stabeno, P. J. and Reed, R. K.: Circulation in the Bering Sea Basin Observed by Satellite-Tracked Drifters: 1986–1993, J. Phys. Oceanogr., 24, 848–854, https://doi.org/10.1175/1520-0485(1994)024< 0848:CITBSB>2.0.CO;2, 1994.

Stein, R., Matthiessen, J., Niessen, F., Krylov, A., Nam, S.-I., and Bazhenova, E.: Towards a better (litho-) stratigraphy and reconstruction of Quaternary paleoenvironment in the Amerasian Basin (Arctic Ocean), Polarforschung, 79, 97–121, 2010.

Stein, R., Fahl, K., Schreck, M., Knorr, G., Niessen, F., Forwick, M., Gebhardt, C., Jensen, L., Kaminski, M., and Kopf, A.: Evidence for ice-free summers in the late Miocene central Arctic Ocean, Nat. Commun., 7, 11148, https://doi.org/10.1038/ncomms11148, 2016.

Su, L., Ren, J., Sicre, M. A., Bai, Y., Zhao, R., Han, X., Li, Z., Jin, H., Astakhov, A. S., Shi, X., and Chen, J.: Changing sources and burial of organic carbon in the Chukchi Sea sediments with retreating sea ice over recent centuries, Clim. Past, 19, 1305-1320, 10.5194/cp-19-1305-2023, 2023.

Su, L., Ren, J., Sicre, M.-A., Bai, Y., Jalali, B., Li, Z., Jin, H., Astakhov, A. S., Shi, X., and Chen, J.: HBIs and Sterols in Surface Sediments Across the East Siberian Sea: Implications for Palaeo Sea-Ice Reconstructions, Geochem. Geophys. Geosyst., 23, e2021GC009940, https://doi.org/10.1029/2021GC009940, 2022.

Tedesco, L., Vichi, M., and Scoccimarro, E.: Sea-ice algal phenology in a warmer Arctic, Sci. Adv., 5, eaav4830, https://doi.org/10.1126/sciadv.aav4830, 2019.

Tolosa, I., Fiorini, S., Gasser, B., Martín, J., and Miquel, J. C.: Carbon sources in suspended particles and surface sediments from the Beaufort Sea revealed by molecular lipid biomarkers and compound-specific isotope analysis, Biogeosciences, 10, 2061–2087, https://doi.org/10.5194/bg-10-2061-2013, 2013.

Volkman, J. K.: A review of sterol markers for marine and terrigenous organic matter, Organ. Geochem., 9, 83–99, https://doi.org/10.1016/0146-6380(86)90089-6, 1986.

Volkman, J. K.: Sterols in Microalgae, edited by: Borowitzka, M. A., Beardall, J., and Raven, J. A., The Physiology of Microalgae, Springer International Publishing, Cham, 485–505, 2016.

Walsh, J. E., Fetterer, F., Scott stewart, J., and Chapman, W. L.: A database for depicting Arctic sea ice variations back to 1850, Geogr. Rev., 107, 89–107, https://doi.org/10.1111/j.1931-0846.2016.12195.x, 2017.

Weingartner, T. J., Danielson, S., Sasaki, Y., Pavlov, V., and Kulakov, M.: The Siberian Coastal Current: A wind- and buoyancy-forced Arctic coastal current, J. Geophys. Res.-Oceans, 104, 29697–29713, https://doi.org/10.1029/1999JC900161, 1999.

Weingartner, T., Aagaard, K., Woodgate, R., Danielson, S., Sasaki, Y., and Cavalieri, D.: Circulation on the north central Chukchi Sea shelf, Deep Sea Res. Pt. II, 52, 3150–3174, https://doi.org/10.1016/j.dsr2.2005.10.015, 2005.

Welschmeyer, N. A.: Fluorometric analysis of chlorophyll a in the presence of chlorophyll *b* and pheopigments, Limnol. Oceanogr., 39, 1985–1992, https://doi.org/10.4319/lo.1994.39.8.1985, 1994.

Williford, K. H., Ward, P. D., Garrison, G. H., and Buick, R.: An extended organic carbon-isotope record across the Triassic–Jurassic boundary in the Queen Charlotte Islands, British Columbia, Canada, Palaeogeogr. Palaeocl., 244, 290–296, https://doi.org/10.1016/j.palaeo.2006.06.032, 2007.

Woodgate, R. A. and Peralta-Ferriz, C.: Warming and Freshening of the Pacific Inflow to the Arctic From 1990–2019 Implying Dramatic Shoaling in Pacific Winter Water Ventilation of the Arctic Water Column, Geophys. Res. Lett., 48, e2021GL092528, https://doi.org/10.1029/2021GL092528, 2021.

Woodgate, R. A. and Aagaard, K.: Revising the Bering Strait freshwater flux into the Arctic Ocean, Geophys. Res. Lett., 32, L02602, https://doi.org/10.1029/2004GL021747, 2005.

Woodgate, R. A., Aagaard, K., and Weingartner, T. J.: A year in the physical oceanography of the Chukchi Sea: Moored measurements from autumn 1990–1991, Deep Sea Res. Pt. II, 52, 3116–3149, https://doi.org/10.1016/j.dsr2.2005.10.016, 2005.

Woodgate, R. A.: Increases in the Pacific inflow to the Arctic from 1990 to 2015, and insights into seasonal trends and driving mechanisms from year-round Bering Strait mooring data, Prog. Oceanogr., 160, 124–154, https://doi.org/10.1016/j.pocean.2017.12.007, 2018.

Xiao, X., Fahl, K., Müller, J., and Stein, R.: Sea-ice distribution in the modern Arctic Ocean: Biomarker records from trans-Arctic Ocean surface sediments, Geochim. Cosmochim. Ac., 155, 16–29, https://doi.org/10.1016/j.gca.2015.01.029, 2015.

Yunker, M. B., Macdonald, R. W., Veltkamp, D. J., and Cretney, W. J.: Terrestrial and marine biomarkers in a seasonally ice-covered Arctic estuary – integration of multivariate and biomarker approaches, Mar. Chem., 49, 1–50, https://doi.org/10.1016/0304-4203(94)00057-K, 1995.

Zhuang, Y., Jin, H., Chen, J., Ren, J., Zhang, Y., Lan, M., Zhang, T., He, J., and Tian, J.: Phytoplankton Community Structure at Subsurface Chlorophyll Maxima on the Western Arctic Shelf: Patterns, Causes, and Ecological Importance, J. Geophys. Res.-Biogeo., 125, e2019JG005570, https://doi.org/10.1029/2019JG005570, 2020.